

4.03 Fracture and Frictional Mechanics: Theory

Y Fialko, University of California San Diego, La Jolla, CA, USA

© 2015 Elsevier B.V. All rights reserved.

4.03.1	Introduction	74
4.03.2	Linear Elastic Fracture Mechanics	74
4.03.2.1	Singular Crack Models	75
4.03.2.2	Planar Breakdown Zone Models	75
4.03.3	The Governing Equations	77
4.03.4	Exact Solutions for Quasistatic Two-Dimensional Planar Cracks	77
4.03.5	Shear Cracks Governed by Rate-and-State Friction Laws	80
4.03.6	Dynamic Effects	81
4.03.7	Fracture Energy	83
4.03.8	Coupling between Elastodynamics and Shear Heating	85
4.03.9	Conclusions	88
	Acknowledgments	89
	References	89

Nomenclature			
\Re		\Re	Real part of a complex argument
ϵ	Small distance	R^*	Dynamic length of the process zone at the crack tip
\bar{D}	Average fault slip	r_0	Effective radius of the crack tip
$f_{ij}(\vartheta)$	Azimuthal dependence of a near-tip stress field	S	Minor axis of an elliptical cavity
\hat{T}	Temperature scale	S_f	Boundary between elastically and inelastically deforming materials
\bar{w}	Nondimensional width of the fault slip zone	T	Temperature
σ_{ij}^0	Stress tensor prior to crack propagation	t	Time
σ_{ij}^1	Stress tensor after crack propagation	U_e	Elastic strain energy
A	Rupture area	U_f	Frictional losses
c	Specific heat	U_G	Fracture energy
$D(x)$	Fault slip	u_i	Displacement vector
D_c	Critical weakening displacement	U_l	Potential energy of remotely applied stresses
D_m	Maximum coseismic displacement	U_r	Radiated energy
F	Half-length of a developed part of a crack on which friction has dropped to a residual level σ_d	V_l	Limiting rupture velocity
f_i	Body force	V_p	P -wave velocity
f_s	Coefficient of static friction	V_r	Rupture velocity
G	Release rate of mechanical energy (per unit crack length)	V_s	S -wave velocity
G_c	Effective fracture energy (per unit crack length)	w	Half-width of the fault slip zone
\Im	Imaginary part of a complex argument	$x, y, z(x_1, x_2, x_3)$	Spatial coordinates
K	Stress intensity factor	α	Nondimensional factor
K_c	Critical stress intensity factor, fracture toughness	γ	Nondimensional factor
L	Crack half-length or full length of a self-healing pulse	δ_{ij}	Kronecker delta function
L^*	Dynamic pulse length	ΔS_1	Surface bounding a prospective increment of the process zone at the crack tip in the result of crack growth
L_c	Critical crack length	ΔS_2	Surface bounding a prospective decrement of the process zone at the crack tip in the result of crack growth
M_0	Scalar seismic moment	ΔU_p	Change in the potential energy
p	Pore fluid pressure	δW	Work done by external forces
Q	Rate of heat generation	$\Delta \sigma$	Stress drop
R	Length of the process zone at the crack tip	ϵ_{ij}	Strain tensor
r	Distance to the crack tip	θ	Nondimensional temperature
		κ	Thermal diffusivity

μ	Shear modulus	σ_n	Normal stress resolved on a fault
ν	Poisson ratio	σ_s	Static strength, or the yield stress in the crack tip process zone
ξ	Dummy variable	σ_t	Shear stress resolved on a fault
ρ	Density	χ	Nondimensional along-crack coordinate
s	Complex variable	ψ	Nondimensional half-length of the developed part of a crack
σ_0	Remotely applied stress	ϕ	Analytic function of a complex argument
σ_d	Residual stress on the developed part of a crack		
σ_{ij}	Stress tensor		

4.03.1 Introduction

Seismic and geodetic observations indicate that most earthquakes are a result of unstable localized shear on quasiplanar faults (Dahlen and Tromp, 1998; Gutenberg and Richter, 1949). Because the thickness of earthquake rupture zones that accommodate slip is much smaller than their characteristic in-plane dimensions, it is natural to idealize earthquake ruptures as shear cracks. Development, propagation, and arrest of shear cracks are subject of the earthquake fracture mechanics. Unlike the engineering fracture mechanics that mainly concerns itself with criteria and details of failure at the tip of tensile cracks propagating through ‘intact’ solids (Freund, 1998; Lawn, 1993), the earthquake fracture mechanics must consider both the inelastic yielding at the rupture fronts and the evolution of friction (in general, rate- and slip-dependent) on the rest of the slipping surface (see Chapters 4.04, 4.05 and 4.06). Although a distinction is sometimes made between the crack models and friction models of an earthquake source (e.g., Kanamori and Brodsky, 2004), the two processes are intrinsically coupled and should be considered jointly. Note that the shear crack propagation does not necessarily imply creation of a new fault in intact rocks, but also refers to slip on a preexisting (e.g., previously ruptured) interface. Mathematically, the crack growth in unbroken media and on preexisting faults is very similar, provided that the slip surface is planar. While shear cracks in unconfined intact media tend to propagate out of their initial planes, such tendency is suppressed at high confining pressures (e.g., Broberg, 1987; Lockner et al., 1992; Melin, 1986), and in the succeeding text, we limit our attention to planar ruptures.

The redistribution of stress and strain due to a spatially heterogeneous fault slip can be described using either kinematic (displacement-controlled boundary conditions) or dynamic (stress-controlled boundary conditions) approach. Kinematic (e.g., dislocation) models are useful if the fault slip is known or can be inferred with sufficient accuracy, for instance, from seismological, geodetic, or geologic observations (Bilby and Eshelby, 1968; Okada, 1985; Savage, 1998; Steketee, 1958; Vvedenskaya, 1959). Dynamic (fracture mechanics) models potentially have a greater predictive power, as they solve for, rather than stipulate, the details of fault slip for given initial stress conditions (Andrews, 1976a; Ben-Zion and Rice, 1997; Burridge and Halliday, 1971; Day, 1982; Freund, 1979; Madariaga, 1976). The time-dependent boundary conditions on the fault are usually deduced by using constitutive laws that relate kinetic friction to the magnitude and velocity of fault slip, preseismic stress, temperature, and other state variables pertinent to the evolution of stress on a

slipping interface. The kinematic and dynamic approaches give rise to identical results for the same slip distribution. Dislocation models are well understood and are widely employed in inversions of seismic and geodetic data for the rupture geometry and spatiotemporal details of slip (e.g., Delouis et al., 2002; Fialko et al., 2005; Hartzell and Heaton, 1983). Fracture mechanics models are intrinsically more complex and less constrained but nonetheless increasingly used to interpret high-quality near-field seismic data (Aochi and Madariaga, 2003; Oglesby and Archuleta, 2001; Peyrat et al., 2001). This chapter will focus on the fracture mechanics approach, and kinematic models will not be discussed. Consequently, the term ‘dynamic’ will be used to describe time-dependent aspects of rupture for which inertial effects are important, that is, in a meaning that is opposite to ‘static’ (rather than ‘kinematic’) descriptions. There exist a number of excellent texts covering the fundamentals of fracture mechanics, with applications to the earthquake source seismology, including Cherepanov (1979), Rice (1980), Rudnicki (1980), Li (1987), Segall (1991), Scholz (2002), and Ben-Zion (2003), among others. This chapter will give an overview of basic aspects of fracture mechanics and some recent theoretical developments.

4.03.2 Linear Elastic Fracture Mechanics

It is well known that structural flaws and discontinuities such as cracks, voids, and inclusions of dissimilar materials give rise to local stress perturbations that may significantly amplify the average applied stress. A classic example is an elliptical cavity in an elastic plate subject to a uniform extension (Inglis, 1913; Lawn, 1993). Provided that the major and minor axes of the cavity are L and S , respectively, the orientation of the remote tensile stress σ_0 is orthogonal to the major axis, and the cavity walls are stress-free, the component of stress parallel to the remote tension assumes a value of $\sigma_0(1 + 2L/S) = \sigma_0(1 + 2\sqrt{L/r})$ at the cavity tip, where $r = S^2/L$ is the radius of the cavity tip. For an extreme case of a sharp slit, $S/L \rightarrow 0$, the stress at the tip scales as $\sigma_0\sqrt{L}/\sqrt{r}$, i.e., becomes unbounded for however small remote loading σ_0 . Full analytic solutions for the stress distribution around sharp cracks (see Section 4.03.4; also, Freund, 1998; Lawn, 1993; Rice, 1968a) indicate that the stress field indeed has a characteristic square root singularity

$$\sigma_{ij}|_{r \rightarrow 0} \approx \frac{K}{\sqrt{2\pi r}} f_{ij}(\vartheta) \quad [1]$$

where $K \sim O(\Delta\sigma\sqrt{L})$ is the stress intensity factor that depends on the crack geometry and loading configuration, $\Delta\sigma$ being the

difference between the far-field stress and stress resolved on the crack walls (hereafter referred to as the stress drop; for an empty crack under remote tension, $\Delta\sigma = \sigma_0$), r is now the distance to the crack tip measured from the crack exterior, and $f_{ij}(\vartheta)$ is a function characterizing the azimuthal dependence of the near-tip stress field (Lawn, 1993; Rice, 1980). Because the governing equations and mathematical structure of solutions are identical for the tensile (mode I), in-plane shear (mode II), and antiplane shear (mode III) cracks (see Section 4.03.4), we will use examples of both tensile and shear cracks to highlight universal features of and important differences between the shear and tensile rupture modes. Such a comparison is instructive because many concepts of fracture mechanics have been developed for tensile failure that is most common in engineering applications and subsequently borrowed for seismologic applications that mostly deal with shear failure. Significant differences in the ambient conditions warrant a careful evaluation of the range of applicabilities of basic assumptions behind the fracture mechanics models (e.g., Rubin, 1993).

4.03.2.1 Singular Crack Models

The square root singularity in the stress field (eqn [1]) is a common feature of all crack models assuming a constant stress drop and elastic deformation of the ambient solid, regardless of the mode of failure, and rupture velocity (as long as the latter remains subsonic, see Section 4.03.5). While this stress singularity is admissible on thermodynamic grounds (in particular, it is integrable, so that the elastic strain energy is finite in any closed volume containing the crack tip), it is clearly unrealistic as no material is able to support infinite stresses. Theoretical arguments supported by a large number of observations suggest that the assumption of a perfect brittle behavior (i.e., elastic deformation of the unbroken host up to the onset of fracture) is violated in some zone around the crack tip (Atkinson, 1987; Irwin, 1957; Lawn, 1993) (Figure 1).

In this zone (commonly referred to as the process or breakdown zone), inelastic yielding prevents stress increases in excess of a certain peak value σ_s that presumably represents the microscopic strength of a material. The size of the process zone r_0 that corresponds to equilibrium (i.e., a crack on a verge of propagating) may be interpreted as the effective radius of the crack tip. Outside of the process zone (at distances $r > r_0$),

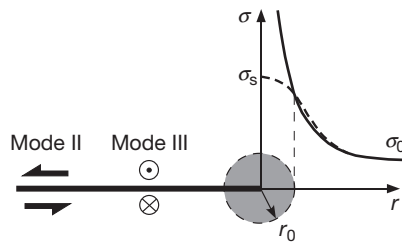


Figure 1 An idealized view of stress variations and yielding at the crack tip. r_0 is the characteristic dimension of a inelastic zone in which stresses exceed the yield threshold σ_s . Solid curve shows the theoretically predicted stress increase with a characteristic $1/\sqrt{r}$ singularity. The theoretical prediction breaks down at distances $r < r_0$ but may be adequate for $r > r_0$.

stresses are below the failure envelope, and the material deforms elastically. If the size of the equilibrium process zone is negligible compared to the crack length, as well as any other characteristic dimensions (e.g., those of an encompassing body), a condition termed small-scale yielding (Rice, 1968a) is achieved, such that the stress and strain fields in the intact material are not appreciably different from those predicted in the absence of a process zone. This is the realm of the linear elastic fracture mechanics (LEFM). According to LEFM, the near-tip ($r_0 < r \ll L$) stress field is completely specified by the scalar multiplier on the singular stress field, the stress intensity factor K (eqn [1]), which can be found by solving an elastic problem for a prescribed crack geometry and loading conditions. The crack propagation occurs when the stress intensity factor exceeds a critical value, $K > K_c$. The critical stress intensity factor, or the fracture toughness K_c , is believed to be a material property, independent of the crack length and loading configuration (although fracture properties may vary for different modes of failure, e.g., K_{Ic} and K_{IIc} , similar to differences between macroscopic tensile and shear strengths). To the extent that the microscopic yield strength σ_s and the effective equilibrium curvature of the crack tip, r_0 , may be deemed physical properties, the fracture toughness K_c may be interpreted as a product $\sigma_s \sqrt{r_0} = \text{const}$.

The critical stress intensity factor is a local fracture criterion, as it quantifies the magnitude of the near-tip stress field on the verge of failure. However, it can be readily related to global parameters characterizing changes in the elastic strain energy ∂U_e and potential energy of applied stresses ∂U_l in the entire body due to a crack extension ∂L , such as the energy release rate $G_c = -(\partial U_e + \partial U_l)/\partial L$,

$$G_c = \frac{\alpha K_c^2}{2\mu} \quad [2]$$

where μ is the shear modulus of an intact material and α assumes values of $(1 - \nu)$ and unity for mode II and mode III loading, respectively (Irwin, 1957). For ideally brittle materials, the energy release rate may be in turn associated with the specific surface energy spent on breaking the intermolecular bonds (Griffith, 1920; Lawn, 1993). Further analysis of the breakdown process at the crack tip requires explicit consideration of the details of stress concentration in the tip region.

4.03.2.2 Planar Breakdown Zone Models

A simple yet powerful extension of the LEFM formulation is the displacement-weakening model, which postulates that (i) the breakdown process is confined to the crack plane, (ii) inelastic deformation begins when stresses at the crack tip reach some critical level σ_s , and (iii) yielding is complete when the crack wall displacement exceeds some critical value D_c (Barenblatt, 1959; Dugdale, 1960; Leonov and Panasyuk, 1959). In case of tensile (mode I) cracks, σ_s represents the local tensile strength in the breakdown zone, and D_c is the critical opening displacement beyond which there is no cohesion between the crack walls. In case of shear (modes II and III) cracks (Figure 2), σ_s represents either the shear strength (for ruptures propagating through an intact solid) or the peak static friction (for ruptures propagating along a preexisting fault), and D_c is the

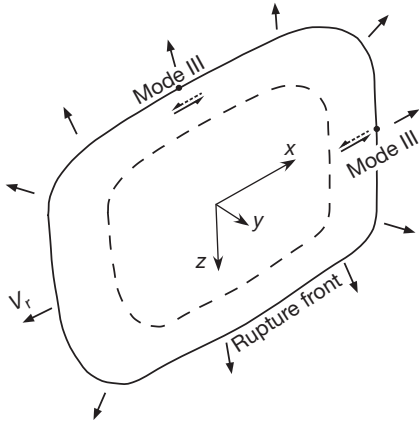


Figure 2 Schematic view of a shear rupture expanding at a constant velocity V . Conditions corresponding to the two-dimensional mode II and mode III loading are approximately satisfied at the rupture fronts orthogonal and parallel to the local slip vector, respectively. For a cracklike rupture, slip occurs on the entire area bounded by the rupture front. For a pulse-like rupture, slip is confined to an area between the rupture front (solid line) and a trailing healing front (dashed line).

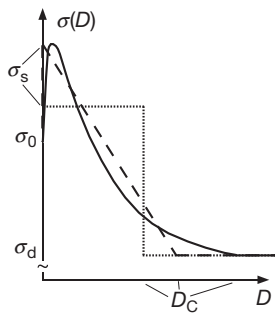


Figure 3 Possible dependence of the breakdown stress σ on the crack wall displacement D within the crack tip process zone. Solid line: a schematic representation of the experimentally measured displacement-weakening relations for rocks (Hashida et al., 1993; Li, 1987). Dashed and dotted lines: approximations of the displacement-weakening relation assuming no dependence of the yield stress on D (dotted line) and linear weakening (dashed line). The area beneath all curves is the same and equals to the fracture energy $G_c = \alpha \sigma_s D_c$, where α is a numerical factor that depends on the particular form of the displacement-weakening relationship. For example, $\alpha = 1$ for the constant yield stress model, and $\alpha = 0.5$ for the linear weakening model.

slip-weakening distance at which a transition to the kinetic friction is complete (Ida, 1972; Palmer and Rice, 1973). Under these assumptions, the fracture energy may be defined as work required to evolve stresses acting on the crack plane from σ_s to the residual value σ_d and is of the order of $(\sigma_s - \sigma_d) D_c$, depending on the details of the displacement-weakening relation (Figure 3). For an ideal brittle fracture that involves severing of intermolecular bonds ahead of the crack tip, σ_s may approach theoretical strength, $\mu/10 \sim O(10^9 - 10^{10} \text{ Pa})$, and D_c may be of the order of the crystal lattice spacing ($10^{-10} - 10^{-9} \text{ m}$), yielding $G_c \sim O(1 \text{ J m}^{-2})$. This is close to the experimentally measured fracture energies of highly brittle crystals and glasses (Griffith, 1920; Lawn, 1993). At the same time, laboratory measurements of polycrystalline aggregates (such as

rocks, ceramics, and metals) reveal much higher fracture energies ranging from $10 - 10^2 \text{ J m}^{-2}$ (for tensile failure) to 10^3 J m^{-2} (for shear failure), presumably reflecting dependence of the effective D_c on the material microstructure (e.g., texture, grain size, and distribution of inhomogeneities) and the breakdown mechanism (e.g., grain unlocking, ligamentary bridging, plasticity, off-plane yielding, or some other deviations from the ideally brittle behavior) (Fialko and Rubin, 1997; Hashida et al., 1993; Li, 1987). Indirect inferences of fracture energies associated with *in situ* propagation of tensile cracks such as man-made hydrofractures and magmatic dikes (Rubin, 1993) and earthquake ruptures (Abercrombie and Rice, 2005; Chester et al., 2005; Hussein, 1977; Wilson et al., 2004) reveal significantly larger fracture energies compared with those measured in the laboratory experiments. This disagreement may be indicative of some scaling of fracture energy with the rupture size or rupture history and perhaps the significance of dynamic effects on cracking and damage that are not captured in laboratory tests. In the context of an in-plane breakdown zone model, the inferred scale dependence of fracture energy is usually interpreted in terms of increases in the effective weakening displacement D_c with the rupture length L . Possible mechanisms of scale dependence of D_c include continued degradation of the dynamic fault strength with slip (e.g., due to thermal or rheological weakening) (Abercrombie and Rice, 2005; Brodsky and Kanamori, 2001; Di Toro et al., 2004; Lachenbruch, 1980) or fractal nature of the fault roughness (e.g., Barton, 1971; Power and Tullis, 1995). It should be pointed out that the common interpretation of the scale dependence of G_c in terms of the scale dependence of D_c may be too simplistic, as the assumption of a thin process zone unlikely holds under *in situ* stress conditions for either tensile or shear cracks, as suggested by both theoretical arguments (Fialko and Rubin, 1997; Poliakov et al., 2002; Rice et al., 2005; Rubin, 1993) and observations (Chester et al., 2005; Fialko, 2004b; Fialko et al., 2002; Manighetti et al., 2001; Wilson et al., 2004). A more detailed quantitative treatment of the energetics of fracture and breakdown processes is presented in Section 4.03.7.

Nonsingular crack models postulating a thin in-plane process zone are mathematically appealing because they allow one to treat the fracture problem as an elastic one by removing nonlinearities associated with failure from the governing equations and incorporating them into boundary conditions on a crack plane. For example, elastic solutions can be readily used to determine the size of the process zone at the crack tip. Dimensional arguments indicate that the strain associated with the material breakdown is of the order of D_c/R , where R is the characteristic size of the breakdown zone. This strain must be of the order of the elastic strain associated with the strength drop, $(\sigma_s - \sigma_d)/\mu$, implying

$$R = \gamma \frac{\mu}{\sigma_s - \sigma_d} D_c \quad [3]$$

where γ is a nondimensional factor of the order of unity that depends on the displacement-weakening relation (e.g., as shown in Figure 3). The small-scale yielding condition requires $R \ll L$. Parallels may be drawn between the size of the breakdown zone R in the displacement-weakening model and the critical radius of the crack tip r_0 in the LFM model

(Figure 1; also, see Khazan and Fialko, 1995), in that both parameters demarcate the near-tip region that undergoes failure from the rest of the material in which the deformation is essentially elastic. On a larger scale, the assumption of elasticity postulates a direct proportionality between the stress drop $\Delta\sigma$ and the average fault slip \bar{D} :

$$\bar{D} \sim \frac{\Delta\sigma}{\mu} L \quad [4]$$

where L is the characteristic fault dimension (for isometric ruptures) or the least dimension of the slip area (in case of ruptures having irregular shape or high aspect ratios). The assumption of a predominantly elastic behavior of the Earth's crust appears to be in a good agreement with seismic (Aki and Richards, 1980; Gutenberg and Richter, 1949; Vvedenskaya, 1959) and geodetic (Fialko, 2004b; Reid, 1910) observations of the instantaneous response of crustal rocks to major earthquakes. The brittle–elastic model gives rise to several fundamental scaling relationships used in earthquake seismology. For example, the scalar seismic moment M_0 is a measure of the earthquake size:

$$M_0 = \bar{D} A \mu \quad [5]$$

where A is the rupture area (Aki, 1967; Kostrov, 1974; also, see Chapter 4.02). The seismic moment is related to a coseismic change in the potential energy of elastic deformation ΔU_e (e.g., Kanamori, 2004),

$$\Delta U_e = \frac{\Delta\sigma}{2\mu} M_0 \quad [6]$$

For isometric ruptures, $A \sim L^2$, and by combining eqns [4] and [5], one obtains a well-known scaling between the scalar seismic moment, the rupture size, and the stress drop (e.g., Dahlen and Tromp, 1998; Kanamori and Anderson, 1975, Chapter 4.02):

$$M_0 \sim \Delta\sigma L^3 \quad [7]$$

4.03.3 The Governing Equations

Consider a three-dimensional medium which points are uniquely characterized by Cartesian coordinates x_i ($i = 1, 2, 3$) in some reference state prior to the fault-induced deformation. Fault slip gives rise to a displacement field u_i . The displacements u_i are in general continuous (differentiable), except across the slipped part of the fault. The strain tensor is related to the displacement gradients as follows:

$$\epsilon_{ij} = \frac{1}{2} (u_{i,j} + u_{j,i}) \quad [8]$$

where the comma operator as usual denotes differentiation with respect to spatial coordinates, $a_{,i} = \partial a / \partial x_i$. Equation [8] assumes that strains are small ($\epsilon_{ij} \ll 1$), so that terms that are quadratic in displacement gradients can be safely neglected (e.g., Landau and Lifshitz, 1986; Malvern, 1969). The assumption of an infinitesimal strain implies no difference between the material (Lagrangian) and spatial (Eulerian) reference frames. Typical strains associated with earthquake ruptures

are of the order of 10^{-4} – 10^{-5} (Kanamori and Anderson, 1975; Scholz, 2002) so that the infinitesimal strain approximation is likely justified. For sufficiently small strain changes (with respect to some reference state), laboratory data and theoretical arguments suggest a linear dependence of strain perturbation on the causal stress change. For an isotropic homogeneous elastic material, the corresponding relationship between stresses and strains is given by Hooke's law (e.g., Landau and Lifshitz, 1986; Timoshenko and Goodier, 1970):

$$\epsilon_{ij} = \frac{1}{2(1+\nu)\mu} [(1+\nu)\sigma_{ij} - \nu\delta_{ij}\sigma_{kk}] \quad [9]$$

where μ and ν are the shear modulus and Poisson's ratio, respectively, δ_{ij} is the Kronecker delta function, and repeating indexes imply summation.

Conservation of a linear momentum in continuous media gives rise to the Navier–Cauchy equations of equilibrium (Malvern, 1969):

$$\sigma_{ij,j} + f_i = \frac{\partial^2 u_i}{\partial t^2} \quad [10]$$

where f_i is the body force (e.g., due to gravity) and t is time. Due to the linearity of equilibrium equations [10], it is possible to represent the full stress tensor as a superposition of some background (e.g., lithostatic and regional tectonic) stress and a perturbation due to fault slip, such that the latter satisfies a homogeneous case of eqns [10]. Unless noted otherwise, in the succeeding text, we assume that the stress tensor σ_{ij} denotes only stress perturbations due to fault displacements. For convenience, the indicial nomenclature for spatial coordinates (x_1, x_2, x_3) will be used interchangeably with the traditional component notation (x, y, z) throughout the rest of the text.

In order to close the problem formulation, some constitutive law relating slip D , slip velocity $\partial D / \partial t$, resolved shear and normal stresses, σ_t and σ_n , pore fluid pressure p , temperature T , etc. needs to be prescribed on surfaces that violate assumptions of continuity, for example, faults and cracks. Examples are the Mohr–Coulomb (Byerlee, 1978) and rate-and-state friction (see Chapter 4.04), flash melting (Molinari et al., 1999; Rice, 2006), thermal pressurization (Andrews, 2002; Segall and Rice, 1995; Sibson, 1973), viscous rheology (Fialko and Khazan, 2005), etc.

4.03.4 Exact Solutions for Quasistatic Two-Dimensional Planar Cracks

In case of two-dimensional deformation (e.g., plane or antiplane strain or plane stress), elastic solutions for stresses and displacements can be generally expressed in terms of two analytic functions of a complex variable $\zeta = x + iy$ (Kolosofov, 1909; Muskhelishvili, 1953). For simplicity, here, we consider loading that is symmetric about the center of the crack $x=0$. In this case, both stresses σ_{ij} and displacements u_i can be expressed through a single analytic function $\phi(\zeta)$ (Westergaard, 1939). First, we demonstrate that the mathematical structure of solutions for stresses and displacements in the crack plane ($y=0$) is identical for tensile (mode I), in-plane shear (mode II), and antiplane shear (mode III) cracks. In particular, for tensile

(mode I) cracks, stresses and displacements can be found from $\phi(\zeta)$ as (e.g., Khazan and Fialko, 2001; Muskhelishvili, 1953)

$$\sigma_{yy} = 2(\Re\phi' + \gamma\Im\phi'') \quad [11]$$

$$\sigma_{xy} = -2\gamma\Re\phi'' \quad [12]$$

$$u_y = \frac{1}{\mu}(2(1-\nu)\Im\phi - \gamma\Re\phi') \quad [13]$$

where \Re and \Im denote the real and imaginary parts of a complex argument. For plane strain shear (mode II) cracks, conditions of symmetry imply that $\sigma_{yy} = 0$ on the crack plane ($y=0$), and the corresponding equilibrium equations are

$$\sigma_{xy} = -2(\Im\phi' + \gamma\Re\phi'') \quad [14]$$

$$u_x = \frac{1}{\mu}(2(1-\nu)\Re\phi + \Im\phi) \quad [15]$$

Upon making a substitution $\phi = -i\phi_1$, one can see that the unknown shear stress σ_{xy} and displacement u_x on the crack plane may be expressed through a new function ϕ_1 in the same manner as the normal stress σ_{yy} and displacement u_y are expressed through ϕ (eqns [11] and [13]),

$$\sigma_{xy} = 2(\Re\phi_1' - \gamma\Im\phi_1'') \quad [16]$$

$$u_x = \frac{1}{\mu}(2(1-\nu)\Im\phi_1 - \gamma\Re\phi_1') \quad [17]$$

For antiplane shear (mode III) cracks, expressions for the relevant stress and displacement components are

$$\sigma_{yz} = -\Im\phi' \quad [18]$$

$$u_z = \frac{1}{\mu}\Re\phi \quad [19]$$

Upon making a substitution $\phi = -2i\phi_2$, one can see that the dependence of the unknown quantities σ_{yz} and $(1-\nu)u_z$ on the analytic function ϕ_2 is analogous to the dependence of σ_{xy} and u_x on ϕ_1 obtained for the in-plane shear crack for $\gamma=0$ (eqns [16]–[17]). This analogy mandates that the mathematical structure of solutions for the tensile, in-plane, and antiplane components of stress for the corresponding crack modes is identical, provided that the boundary conditions on the crack plane (the along-crack distribution of the driving stress and the displacement-weakening relationship) are analogous. Solutions for the crack wall displacements are also identical for different modes, although expressions for displacements for mode III cracks will differ from those for mode I and mode II cracks by a factor of $(1-\nu)$. Hence, we focus on a particular case of an in-plane shear (mode II) crack. The boundary conditions for the potential function ϕ_1 are as follows:

$$\Re\phi_1' = \sigma(x)/2 \quad \text{for } |x| < L \quad [20]$$

$$\Im\phi_1' = 0 \quad \text{for } |x| > L \quad [21]$$

$$\phi_1' \rightarrow \sigma_0/2 \quad \text{for } |\zeta| \rightarrow \infty \quad [22]$$

where $\sigma(x)$ is the distribution of shear stress on the crack surface and σ_0 is the applied shear stress at infinity (hereafter referred to as prestress). The boundary condition [21] postulates no slip beyond the rupture front (see eqn [17]). An explicit solution for the function ϕ_1 that is analytic in the upper half plane and satisfies the boundary conditions [20]–[22] is given by the

Keldysh–Sedov formula (Gakhov, 1966; Khazan and Fialko, 1995, 2001; Muskhelishvili, 1953):

$$\phi_1'(\zeta) = \frac{1}{2\pi i} \left(\frac{\zeta+L}{\zeta-L} \right)^{1/2} \int_{-L}^L d\xi \left(\frac{\xi-L}{\xi+L} \right)^{1/2} \frac{\sigma(\xi)}{\xi-\zeta} + \frac{\sigma_0}{2} \left(\frac{\zeta+L}{\zeta-L} \right)^{1/2} + \frac{C}{(\zeta^2-L^2)^{1/2}} \quad [23]$$

where C is an arbitrary constant. From eqn [16], an asymptotic behavior of ϕ_1' at infinity is

$$\lim_{|\zeta| \rightarrow \infty} \phi_1'(\zeta) = -\frac{1}{2\pi i |\zeta|} \int_{-L}^L d\xi \left(\frac{\xi-L}{\xi+L} \right)^{1/2} \sigma(\xi) + \frac{\sigma_0}{2} + \frac{L\sigma_0 + C}{|\zeta|} \quad [24]$$

One can readily determine the unknown constant C from eqn [16] by satisfying the boundary condition [22]. The final expression for the derivative of analytic function ϕ_1 is

$$\phi_1'(\zeta) = \frac{1}{2\pi i} \left(\frac{\zeta+L}{\zeta-L} \right)^{1/2} \int_{-L}^L d\xi \left(\frac{\xi-L}{\xi+L} \right)^{1/2} \frac{\sigma(\xi)}{\xi-\zeta} + \frac{\sigma_0}{2} \left(\frac{\zeta+L}{\zeta-L} \right)^{1/2} + \frac{1}{2\pi(\zeta^2-L^2)^{1/2}} \int_{-L}^L d\xi \frac{\sigma(\xi) - \sigma_0}{(L^2 - \xi^2)^{1/2}} \quad [25]$$

For any physically admissible failure model, the maximum stress within the slipped region is bounded by the yield strength, $\sigma_{xy} < \sigma_s$ for $|x| < L$. Furthermore, it is reasonable to expect that $\sigma_{xy} \rightarrow \sigma_s$ as $|x| \rightarrow L$. The shear stress $\sigma_{xy}(\zeta)$ in the ‘locked’ region ahead of the rupture front is then given by the real part of ϕ_1 (see eqn [16]). Sufficiently close to the crack tip (i.e., for $\zeta = L + \epsilon$, such that $\Im\epsilon = 0$, $0 < \epsilon \ll L$), we obtain

$$\sigma_{xy}(L + \epsilon) = \frac{1}{\pi} \left(\frac{L}{2\epsilon} \right)^{1/2} \int_{-L}^L d\xi \frac{\sigma(\xi) - \sigma_0}{(L^2 - \xi^2)^{1/2}} + \sigma_s + O(\epsilon^{1/2}) \quad [26]$$

The first term on the right-hand side of eqn [26] is of the order of $1/\sqrt{\epsilon}$ and represents the LEFM approximation (see Section 4.03.2). By comparing eqns [26] and [1], one can formally introduce the stress intensity factor,

$$K = \frac{1}{\pi} \left(\frac{L}{2\epsilon} \right)^{1/2} \int_{-L}^L d\xi \frac{\sigma(\xi) - \sigma_0}{(L^2 - \xi^2)^{1/2}} \quad [27]$$

which exhibits the expected scaling $K \propto \Delta\sigma\sqrt{L}$. Physically plausible crack models require that stresses are finite everywhere. From eqns [26] and [27], the requirement of the absence of a stress singularity is met if (and only if)

$$\int_{-L}^L d\xi \frac{\sigma(\xi) - \sigma_0}{(L^2 - \xi^2)^{1/2}} = 0 \quad [28]$$

Any realistic distribution of the driving stress resolved the crack surface must satisfy the integral constraint [28]. This implies that the driving stress $(\sigma(x) - \sigma_0)$ must change sign along the crack ($|x| < L$). For example, the stress drop ($\sigma(x) < \sigma_0$) in the central part of the crack needs to be balanced by the material strength or the high transient friction ($\sigma_s \geq \sigma(x) > \sigma_0$) within the process zone.

Displacements of the crack walls $u_x(x)$ corresponding to the instantaneous shear stress $\sigma(x)$ can be found by differentiating equation [17] for $\gamma=0$,

$$\frac{du_x}{dx} = \frac{2(1-\nu)}{\mu} \mathfrak{I}\phi'_1 \quad [29]$$

and making use of expression [26] to integrate the resulting differential equation [29] with the initial condition $u_x(-L)=0$. The respective solution is

$$D(x) = \frac{2(1-\nu)}{\pi\mu} \int_x^L (L^2 - \xi^2)^{1/2} d\xi \int_{-L}^{\xi} \frac{\sigma(t)dt}{(L^2 - t^2)^{1/2}(t - \xi)} \quad [30]$$

where $D(x)=2u_x(x)$ is slip between the crack walls. The problem is closed by specifying a constitutive relationship between slip D and kinetic friction σ . In general, such a relationship may include dependence of friction on slip rate, slip history, local temperature, and other state variables (Dieterich, 1979; Blanpied et al., 1995; Ruina, 1983, Chapters 4.04, 4.05 and 4.06). To gain a further analytic insight, here, we consider a simple slip-weakening relationship

$$\begin{aligned} \sigma(x) &= \sigma_s \text{ for } D(x) < D_c \\ \sigma(x) &= \sigma_d \text{ for } D(x) > D_c \end{aligned} \quad [31]$$

where σ_s is the yield strength or static friction in the process zone, σ_d is the residual kinetic friction on the developed part of the crack, and D_c is the critical slip-weakening displacement corresponding to a transition from σ_s to σ_d (see Figure 3). The size of the process zone, R , is defined by a requirement that the fault slip is subcritical within the process zone, $D(|F|)=D_c$, where $F=L-R$ is the length of the developed part of a crack on which the friction has dropped to a residual value σ_d . Figure 4 illustrates the geometry of the problem. In case of a piece-wise constant distribution of shear stress along the crack $\sigma(x)$ given by eqn [32], as shown in Figure 4, expressions [28] and [30] can be readily integrated to provide closed form analytic solutions. In particular, integration of expression [28] allows one to determine a relative size of the process zone with respect to the crack half-length:

$$\frac{R}{L} = 2\sin^2\left(\frac{\pi}{4} \frac{\sigma_0 - \sigma_d}{\sigma_s - \sigma_d}\right) \quad [32]$$

Evaluation of integral [30] gives rise to

$$D(x) = \frac{2(1-\nu)L}{\pi\mu} (\sigma_0 - \sigma_d) I(\chi, \psi) \quad [33]$$

where $\chi=x/L$ and $\psi=F/L$ are the nondimensional along-crack coordinate and the half-length of the developed part of the crack, respectively, and function I is given by the following equation:

$$\begin{aligned} I(U, V) &= (V+U) \log \left| \frac{1+UV + \sqrt{(1-U^2)(1-V^2)}}{V+U} \right| \\ &+ (V-U) \log \left| \frac{1-UV + \sqrt{(1-U^2)(1-V^2)}}{V-U} \right| \end{aligned} \quad [34]$$

At the base of the process zone, $\chi=\psi$, eqn [33] reduces to

$$D(F) = \frac{4(1-\nu)}{\pi\mu} F(\sigma_s - \sigma_d) \log \frac{1}{\psi} \quad [35]$$

For a crack that is on the verge of propagating, slip at the base of the process zone ($x=F$) equals the critical weakening displacement D_c . A simple dimensional analysis of eqn [35] then reveals a characteristic length scale L_c :

$$L_c = \frac{\pi D_c}{4(1-\nu)} \frac{\mu}{\sigma_s - \sigma_d} \quad [36]$$

Using eqn [36], eqn [35] may be written

$$\frac{L_c}{F} = \log \frac{L}{F} \quad [37]$$

A further rearrangement of eqn [37] yields an explicit expression for the length of the process zone R :

$$R = F \left(\exp\left(\frac{L_c}{F}\right) - 1 \right) \quad [38]$$

It is instructive to consider two end-member cases, the long crack limit, $F \gg L_c$, and the microcrack limit, $F \ll L_c$. In case of sufficiently long cracks ($F \gg L_c$), an asymptotic expansion of eqn [38] (i.e., $\exp(x) \approx 1+x$ for $x \ll 1$) indicates that the process zone length is independent of the crack length and equals L_c . This is the realm of small-scale yielding, $R = \text{const} = L_c \ll L$, $F \approx L$, in which cracks propagate by preserving the structure of the near-tip stress field. By comparing eqns [37] and [3], one can see that the general scaling relationship suggested by dimensional arguments holds; for the case of a constant breakdown stress σ_s within the process zone, the nondimensional coefficient γ in estimate [3] equals $\pi/4(1-\nu)$. Exact analytic solutions assuming small-scale yielding give rise to $\gamma = \pi/2(1-\nu)$ for a linear slip-weakening relationship (see Figure 3) (e.g., Chen and Knopoff, 1986) and $\gamma = 9\pi/16(1-\nu)$ for a breakdown stress that linearly decreases with distance away from the crack tip (Palmer and Rice, 1973). In the microcrack limit, the length of the equilibrium process zone is not constant even if the critical weakening displacement D_c and the strength drop $(\sigma_s - \sigma_d)$ are intrinsic material properties

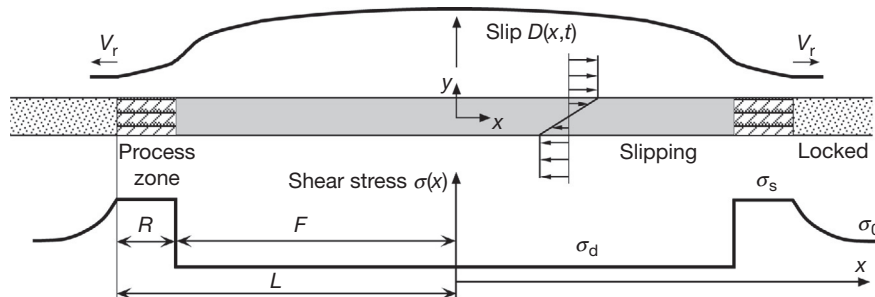


Figure 4 A two-dimensional plain strain shear crack in an infinite elastic medium. The imposed shear stress at the infinity is σ_0 . The developed part of the crack is assumed to have a constant residual shear stress σ_d . At the crack tips, there are process zones having length R and shear stress σ_s .

independent of the ambient stress and loading conditions. In particular, R is predicted to exponentially increase as the length of the stress drop region F decreases. Equations [38] and [32] suggest that the presence of sufficiently short cracks (such that $F < L_c$) has no effect on the macroscopic ‘strength’ of rocks. In particular, the prestress required for the crack extension must approach the static yield limit, $\sigma_0 \rightarrow \sigma_s$, and the size of the yield zone increases without bound, $L \approx R \rightarrow \infty$, for $F \rightarrow 0$ (see eqn [38]).

Quantitative estimates of the critical length scale L_c are not straightforward because it is not clear whether the slip-weakening distance D_c is indeed a scale-independent material constant (e.g., Barton, 1971; Ohnaka, 2003; Rudnicki, 1980). Laboratory measurements of the evolution of friction on smooth slip interfaces indicate that D_c may be of the order of 10^{-5} m (Dieterich, 1979; Li, 1987; Marone, 1998). For $\mu \sim 10^{10}$ Pa and $(\sigma_s - \sigma_d) \sim 10^7 - 10^8$ Pa (likely spanning the range of strength drops for both ‘strong’ and ‘weak’ faults), from eqn [36], one obtains $L_c \sim 10^{-3} - 10^{-1}$ m, negligible compared to the characteristic dimension of the smallest recorded earthquakes but comparable to the typical sample size used in the laboratory experiments. An upper bound on L_c may be obtained from estimates of the effective fracture energies of earthquake ruptures. For large (moment magnitude > 6) earthquakes, the seismically inferred fracture energies $G_c = (\sigma_s - \sigma_d)D_c$ are of the order of $10^6 - 10^7$ J m $^{-2}$ (Abercrombie and Rice, 2005; Beroza and Spudich, 1988; Husseini, 1977; Ida, 1972), rendering the effective $D_c \sim 0.01 - 1$ m. Assuming that the seismically inferred values of D_c are applicable to quasistatic cracks, eqn [36] suggests that a transition from ‘micro’ to ‘macro’ rupture regimes occurs at length scales of the order of $1 - 10^3$ m.

The magnitude of a prestress required to initiate the crack propagation can be found by combining eqns [37] and [32]:

$$\frac{\sigma_s - \sigma_0}{\sigma_s - \sigma_d} = \frac{2}{\pi} \arcsin \exp\left(-\frac{L_c}{F}\right) \quad [39]$$

In the microcrack or large-scale yielding limit, $F \ll L_c$, eqn [39] predicts $\sigma_0 \approx \sigma_s$, that is, the crack propagation requires ambient stress comparable to the peak static strength of crustal rocks, as discussed in the preceding text. In the small-scale yielding limit, $F \gg L_c$, eqn [39] gives rise to a well-known inverse proportionality between the stress drop $(\sigma_0 - \sigma_d)$ and the square root of the crack length F (e.g., Cowie and Scholz, 1992; Kostrov, 1970; Rice, 1968a):

$$\sigma_0 = \sigma_d + \frac{2}{\pi} (\sigma_s - \sigma_d) \left(\frac{2L_c}{F}\right)^{1/2} \quad [40]$$

It follows from eqn [40] that for sufficiently large ruptures, the background tectonic stress required for the rupture propagation does not need to appreciably exceed the residual friction on the slipped surface σ_d . That is, the stress drop associated with the rupture propagation, $(\sigma_0 - \sigma_d)$, may be much smaller than the strength drop, $(\sigma_s - \sigma_d)$, provided that the rupture size significantly exceeds the critical nucleation size L_c . This statement forms the basis of the ‘statically strong, but dynamically weak’ fault theory (Lapusta and Rice, 2004). According to this theory, major crustal faults may operate at relatively low driving stresses (e.g., sufficient to explain the so-called heat flow paradox of the San Andreas fault (Brune et al., 1969;

Lachenbruch, 1980)), even if the peak failure stress required for the onset of dynamic weakening is consistent with Byerlee’s law and hydrostatic pore pressures (Byerlee, 1978; Marone, 1998; Scholz, 2002), provided that $\sigma_d \ll \sigma_s$. If so, earthquake ruptures must nucleate in areas where σ_0 approaches σ_s (due to either locally increased ambient stress or decreased static strength, e.g., due to high pore fluid pressures) and propagate into areas of relatively low ambient stress. Under this scenario, the overall fault operation must be such that the average stress drop $\Delta\sigma$ remains relatively small (of the order of 0.1–10 MPa) and essentially independent of the rupture size (Abercrombie, 1995; Kanamori and Anderson, 1975; Scholz, 2002). Because the overall seismic moment release is dominated by the largest events, the implication from the Lapusta and Rice (2004) model is that the Earth crust is not able to support high deviatoric stresses in the vicinity of large active faults. Phenomenologically, this is consistent with the ‘weak fault’ theory maintaining that the average shear stress σ_0 resolved on mature faults is of the order of the earthquake stress drops (i.e., up to a few tens of megapascals) and is considerably less than predictions based on Byerlee’s law (a few hundreds of megapascals) (e.g., Kanamori and Heaton, 2000). The ‘statically strong but dynamically weak’ fault theory seeks to reconcile laboratory results from rock friction experiments with seismic observations. Neither the peak shear stress σ_s nor the residual dynamic friction σ_d can be estimated from seismic data. Both parameters are likely scale-dependent; for example, the peak shear stress σ_s may vary from gigapascals on the scale of microasperities and gouge particles (10^{-6} m) to the Mohr–Coulomb stress $f_s(\sigma_n - p)$, where f_s is the static coefficient of friction, σ_n is the fault-normal stress, and p is the pore fluid pressure, on the scale of centimeters to meters (i.e., consistent with laboratory data), to values that may be lower still on scales of hundreds of meters to kilometers. Similarly, the residual dynamic friction may depend on the amount of slip (and the rupture size) (e.g., Abercrombie and Rice, 2005; Brown and Fialko, 2012; Kanamori and Heaton, 2000; Rice, 2006); implications from such behavior are further discussed in Section 4.03.7.

4.03.5 Shear Cracks Governed by Rate-and-State Friction Laws

More sophisticated models of earthquake faults combine elasticity with empirical friction laws that relate shear stress to normal stress and slip velocity and slip history. In particular, the rate-and-state phenomenology (Dieterich, 1979; Ruina, 1983) provides a system of differential equations that can be used to define shear stress (e.g., σ in eqn [30]) on a fault plane without oversimplifying assumptions, such as eqns [32]. The resulting system of equations precludes analytic solutions, and numerical experiments are required to investigate the evolution of stress and slip rate on a fault. In the framework of rate-and-state friction, material properties that govern fault slip are a (rate parameter), b (state parameter), and the characteristic evolution distance analogous to the critical weakening displacement D_c discussed in the preceding text (e.g., Figure 3; also, see Chapter 4.04).

In particular, numerical simulations performed by Dieterich (1992) revealed that slip instabilities on a

rate-and-state fault require a nucleation zone having a characteristic size greater than $L_b = D_c \mu / [(1 - \nu) b \sigma_n]$, where σ_n is the fault-normal stress (see Figure 4 in Chapter 4.04). The existence of a minimum nucleation length scale was previously suggested based on a conditional stability of a spring-box slider (e.g., Gu et al., 1984; Rice, 1993; Ruina, 1983). However, the spring-box slider model predicts that the minimum nucleation length should scale as $(b - a)^{-1}$, rather than b^{-1} , as reported by Dieterich (1992). This discrepancy may stem from the fact that slip on a deformable fault is intrinsically a higher dimensional (2-D or 3-D) problem compared with a (1-D) problem of motion of a spring-box slider.

Rubin and Ampuero (2005) showed that L_b is in fact the minimum nucleation length and that for a weakly weakening ($a/b \rightarrow 1$, that is, nearly velocity neutral) friction, larger nucleation areas can exist, with the characteristic length of the order of $b^2/(b - a)^2 L_b$. The latter can be reached under quasi-steady-state conditions (such that the state variable is nearly constant), while L_b is the minimum nucleation length when the fault is well above steady state (the state variable is rapidly changing) (Ampuero and Rubin, 2008; Rubin and Ampuero, 2005).

Some parallels may be drawn between the analytic solutions presented in Section 4.03.4 and numerical results for rate-state faults (Ampuero and Rubin, 2008; Dieterich, 1992; Rubin and Ampuero, 2005). If one approximates the velocity change at the tip of a slipping patch on a rate-state fault by a step function (e.g., see Figure 8 in Chapter 4.02), then parameters $a\sigma_n$ and $b\sigma_n$ of rate-and-state friction are analogous to the difference between the yield strength and the background stress ($\sigma_s - \sigma_0$) and the strength drop ($\sigma_s - \sigma_d$), respectively (see Figure 4 in this chapter and Figure 1 in Chapter 4.04). The characteristic length of the process zone L_c (eqn [36]) is then essentially coincident with the minimum nucleation size L_b established by Dieterich (1992) based on numerical simulations coupling the rate-and-state friction and elasticity. The correspondence between the two length scales may be interpreted as indicating that no elastodynamic instability is possible in the microcrack regime ($F < L_c$). On the other hand, a condition $a/b \rightarrow 1$ implies $\sigma_0 \approx \sigma_d$, that is, small-scale yielding (see eqn [40]). Indeed, such conditions were satisfied prior to the onset of elastodynamic instability in numerical experiments of Rubin and Ampuero (2005) performed under the assumption of weak velocity weakening. Using eqns [32] and [38], one can see that in the limit $R/L \ll 1$, $b^2/(b - a)^2 L_c \sim L/R$ $L_c = L$, that is, the 'velocity neutral' nucleation length of Rubin and Ampuero (2005) is essentially the length of a quasistatic crack on the verge of propagation under a constant remote stress σ_0 . This is the maximum length of a slip patch satisfying conditions of a quasistatic equilibrium. The main differences between the rate-state model and that shown in Figure 4 is that the latter assumes a piece-wise constant stress distribution on the crack surface and zero slip velocity ahead of the crack tip, while in the rate-state model, the shear stress is a continuous function of distance along the fault, and the fault slip rate is never zero. This analogy between the analytic solution for a static crack and a deformable rate-state fault may hold because of large (orders of magnitude) increases in the slip velocity at the tip of an accelerating slip patch compared to the nominally locked region ahead of the

tip; variations in slip rate behind the rupture front are much smaller in comparison, so that a steplike change in slip rate may be a reasonable approximation.

4.03.6 Dynamic Effects

Quasistatic solutions considered in Section 4.03.4 are valid only for rupture speeds that are well below the shear wave velocity V_s . As the rupture velocity increases, the inertial term in the equilibrium equations [10] eventually becomes non-negligible, and the near-tip stress field is significantly altered when V_r becomes a sizeable fraction of V_s (Andrews, 1976a; Broberg, 1978; Freund, 1979; Rice, 1980). The most pronounced effects of a high rupture speed are the relativistic shrinking of the in-plane process zone R and simultaneous increase of stress perturbations off the crack plane (Kame and Yamashita, 1999; Poliakov et al., 2002; Rice et al., 2005). The net result is an increased tendency for branching, bifurcation, and nonsteady propagation, all of which significantly complicate the analytic and numerical treatment of the elastodynamic rupture problem. In particular, the intermittent propagation of the rupture front invalidates the equivalence between the LFM and slip-weakening formulations (e.g., Freund, 1979), implying a greater dependence of the model results on a specific choice of fracture criteria.

Analysis of the full elastodynamic equilibrium equations [10] reveals that solutions exist for rupture velocities below a limiting speed V_l , which equals to the Rayleigh wave velocity V_R for mode II cracks and shear wave velocity for mode III cracks (e.g., Freund, 1979; Kostrov and Das, 1988). Solutions become singular as $V_r \rightarrow V_l$; in particular, the dynamic stress intensity factor and the energy release rate at the crack tip asymptotically vanish. Main fracture mechanics parameters of a steady-state elastodynamic rupture (such as the process zone size and the stress intensity factors) may be readily obtained by multiplying or dividing the respective results from quasistatic solutions by dimensionless coefficients that depend on rupture velocity only. The corresponding coefficients are

$$f_{II} = (1 - \nu) \frac{4 \sqrt{1 - \frac{V_r^2}{V_p^2}} \sqrt{1 - \frac{V_r^2}{V_s^2}} - \left(2 - \frac{V_r^2}{V_s^2}\right)^2}{\frac{V_r}{V_s} \sqrt{1 - \frac{V_r^2}{V_s^2}}} \quad [41]$$

$$f_{III} = \sqrt{1 - \frac{V_r^2}{V_s^2}} \quad [42]$$

for the mode II and mode III loading, respectively (e.g., Freund, 1998; Rice, 1980). In eqn [41], V_p is the P-wave velocity. Coefficients f_{II} and f_{III} monotonically decrease from unity at $V_r = 0$ to zero at $V_r = V_l$. For instance, the length of the dynamic process zone R^* is given by $R^*(V_r) = f_{II,III}(V_r)R$, and the dynamic stress intensity factor for a self-similar expanding crack is $K_{II,III}(V_r) = f_{II,III}(V_r)K_{II,III}(0)$. Note that for a steady-state self-healing pulse with a fixed stress distribution in the reference frame of a moving pulse, the process zone shortens at high rupture velocity, similar to the case of a self-similar crack, but the dynamic stress intensity factor is independent of V_r .

Rice et al. (2005) confirmed these results with full analytic solutions for a self-healing pulse with a linearly weakening process zone, propagating at a constant rupture speed. They found that the ratio of the dynamic process zone R^* to the pulse length L^* is independent of the rupture speed but is dependent on the ratio of stress drop to strength drop:

$$\frac{\sigma_0 - \sigma_d}{\sigma_s - \sigma_d} = \frac{\xi}{\pi} - \frac{\xi - \sin \xi}{2\pi \sin^2(\xi/2)} \quad [43]$$

where $\xi = 2 \arcsin \sqrt{R^*/L^*}$ (cf. eqn [32]). The velocity invariance of the relative size of the process zone gives rise to a somewhat unintuitive result that the pulse length L^* vanishes as the rupture accelerates to a limiting speed. At the same time, the amount of slip produced by a self-healing pulse is also invariant with respect to the rupture velocity. Thus, the dynamically shrinking rupture size gives rise to a dramatic increase in the near-field coseismic strain. Figure 5 shows the dependence of the near-tip stress concentration on the rupture speed inferred from the Rice et al. (2005) model. As one can see from Figure 5, the extent of the off-plane yielding and damage substantially increases at high rupture speeds, so that the assumption of a thin in-plane process zone ceases to be valid. Similar results were reported for a semi-infinite crack by Poliakov et al. (2002). Note that the deduced areas of yielding

likely underestimate the extent of off-fault damage, as stresses inside the shaded areas in Figure 5 are beyond the failure envelope. By explicitly allowing inelastic deformation, the excess stresses will be relaxed, and the yielding zone will further expand. The enhanced off-fault damage may be one of the mechanisms preventing extreme contractions of the rupture length at high propagation velocities. It may also appreciably modify the expenditure part of the earthquake energy balance, as discussed in the following section.

Elastodynamic slip instabilities with rupture velocity below the limiting speed V_l are referred to as subsonic or subshear rupture. The majority of earthquakes for which high-quality measurements of the rupture speed are available appear to be subsonic. Theoretical models indicate that immediately above the limiting rupture speed V_l , the flux of mechanical energy into the crack tip region becomes negative for tensile and mode II shear cracks, effectively prohibiting self-sustained fracture (Broberg, 1999; Freund, 1998). However, physically admissible solutions do exist for shear cracks with rupture speeds spanning the interval between the S-wave and P-wave velocities; such mode of propagation is referred to as intersonic, transonic, or supershear rupture (Andrews, 1976b; Broberg, 1989; Burridge, 1973; Simonov, 1983). Although the mechanics of transition from the subsonic ($V_r < V_l$) to transonic

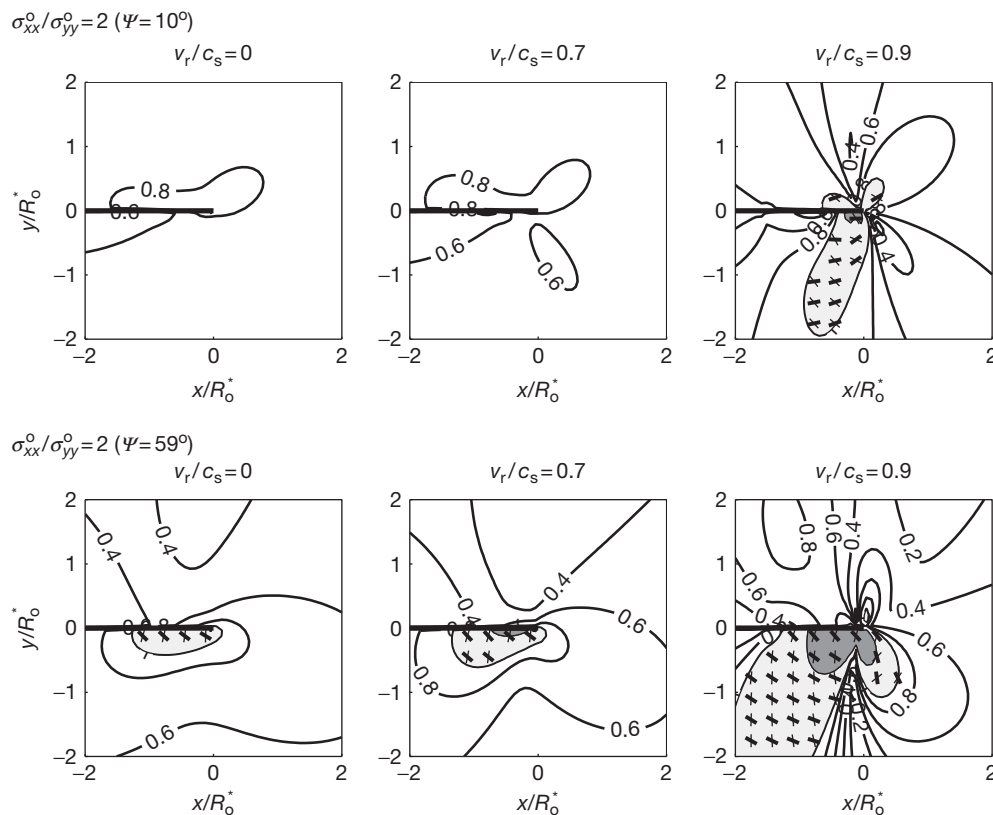


Figure 5 Stress perturbation around the tip of a propagating slip pulse with a linear slip-weakening process zone (reproduced from Rice JR, Sammis CG, and Parsons R (2005) Off-fault secondary failure induced by a dynamic slip pulse. *Bulletin of the Seismological Society of America* 95: 109–134, their Figure 6). Light shading denotes areas where the Mohr–Coulomb failure envelope is exceeded (likely to fail in shear), and dark shading denotes areas of absolute tension (likely to fail by tensile cracking). Thick tick marks indicate the orientation of optimal planes for right-lateral slip, and thin tick marks indicate the orientation of optimal planes for left-lateral slip. Ψ is an angle between the maximum compression axis and the fault plane. Process zone comprises 10% of the rupture length. Axes are normalized by the quasistatic process zone size.

($V_r > V_s$) propagation is not fully understood, there is experimental (Samudrala et al., 2002; Xia et al., 2004) and seismologic (Archuleta, 1984; Bouchon and Vallee, 2003; Dunham and Archuleta, 2004; Wald and Heaton, 1994) evidence that transonic rupture speeds may be achieved under certain conditions. The spatial structure of the near-tip stress field and the radiation pattern in the transonic regime are markedly different from those due to subsonic ruptures (see Chapter 4.08).

4.03.7 Fracture Energy

The concept of fracture energy was originally introduced for tensile cracks by Griffith (1920) to quantify the irreversible work associated with breaking of the intermolecular bonds and creation of a stress-free crack surface. Griffith's definition based on a global energy balance was subsequently shown to be equivalent to local definitions based on the LEFM and small-scale yielding models (Rice, 1968a; Willis, 1967). For example, for a Barenblatt-type process zone model, the fracture energy is the work spent against the cohesive stress σ_s in the process zone on separating the crack walls by the critical opening distance D_c . An elegant demonstration of the equivalence of global and local definitions of fracture energy for tensile cracks was provided by Rice (1968b) in a form of the path-independent J -integral (also, see Cherepanov, 1968; Eshelby, 1956). Palmer and Rice (1973) extended this technique to the case of shear cracks and defined the shear fracture energy as work required to evolve shear stress on the slip interface from the yield stress (or static friction) σ_s to the residual dynamic friction σ_d :

$$G_c = \int_0^{D_c} (\sigma(D) - \sigma_d) dD \quad [44]$$

where $\sigma(D)$ varies between σ_s and σ_d for $0 < D < D_c$, respectively. A similar formulation was introduced by Ida (1972). Equation [44] allows a simple insight into the fracture process and has been widely used for interpretations of seismic data. However, several factors may limit its application to the analysis of earthquake ruptures. First, the displacement-weakening model assumes that all inelastic deformation is limited to the slip plane. Both theoretical models (Andrews, 2005; Rice et al., 2005; Rudnicki, 1980) (Figure 5) and field observations (Chester et al., 2005; Fialko, 2004b; Fialko et al., 2002; Li et al., 1998) suggest that the earthquake-induced damage likely extends well off of the fault plane, and the energy dissipated in the fault damage zone may be quite significant (e.g., Andrews, 2005; Ben-Zion and Shi, 2005; Wilson et al., 2004). Second, the fracture energy given by eqn [44] has a clear physical interpretation if the residual dynamic stress σ_d is constant (or at least if the along-fault variations in σ_d are small compared to the strength drop, $\sigma_s - \sigma_d$). The second point can be illustrated by considering a traditional representation of the earthquake energy budget:

$$\Delta U_p = U_r + U_f + U_G \quad [45]$$

where ΔU_p is the change in the total potential energy (which includes changes in the elastic strain energy ΔU_e and gravitational potential energy); U_r is the energy radiated in seismic

waves; U_f is the energy dissipated on the well-slipped portion of the fault due to friction, comminution, phase transitions, and other irreversible losses; and U_G is the fracture energy spent on overcoming high resisting stresses near the crack tip (Dahlen, 1977; Kostrov, 1974; Rivera and Kanamori, 2005; Rudnicki and Freund, 1981). A significant part of U_f is believed to be ultimately converted into heat (Fialko, 2004a; Sibson, 1980). Under the approximation of the displacement-weakening model, $U_G \propto \sigma_s D_c$ and $U_f \propto \sigma_d D_m$. Assuming that the residual friction is of the order of the peak strength, $\sigma_d \sim O(\sigma_s)$, and the critical slip-weakening distance is much smaller than the coseismic offset, $D_c \ll D_m$, the fracture energy is negligible compared to frictional losses in the earthquake energy balance equation [45]. However, if the fault friction progressively decreases with slip, as suggested by the experimental observations and theoretical inferences of the dynamic weakening (Abercrombie and Rice, 2005; Di Toro et al., 2004; Fialko and Khazan, 2005; Goldsby and Tullis, 2002; Tsutsumi and Shimamoto, 1997), the effective slip-weakening distance D_c is expected to scale with the slip magnitude, and the fracture energy U_G may not be small compared to U_f . Because neither the slip-weakening distance D_c nor the residual friction σ_d in this case are material properties (in particular, they may depend on the details of slip history, thickness and permeability of the slip zone, etc.), a distinction between U_G and U_f terms in the earthquake energy balance equation [45] becomes somewhat arbitrary. Note that for a rupture on a preexisting fault, there is little *physical* difference between U_G and U_f , as both terms represent spatially and temporally variable frictional losses associated with fault slip; both U_G and U_f ultimately contribute to wearing and heating on the slip interface. The situation is further complicated if the dynamic friction is a nonmonotonic function of slip (e.g., Brune and Thatcher, 2002; Hirose and Shimamoto, 2005; Rivera and Kanamori, 2005; Tinti et al., 2005). While a formal distinction between the frictional and fracture losses associated with shear ruptures may be problematic, the entire amount of work spent on inelastic deformation of the host rocks during the crack propagation is unambiguous and can be readily quantified. For simplicity, here, we consider the case of a quasistatic crack growth. Formulation presented in the succeeding text can be also generalized to the case of dynamic cracks.

Consider an equilibrium mode II crack in a medium subject to initial stress σ_{ij}^0 . The medium is elastic everywhere except inside the crack and within a finite process zone near the crack tips (Figure 6(a)). The inelastic zone is demarcated by a surface S_f . Let external forces do some work δW on a medium, in the

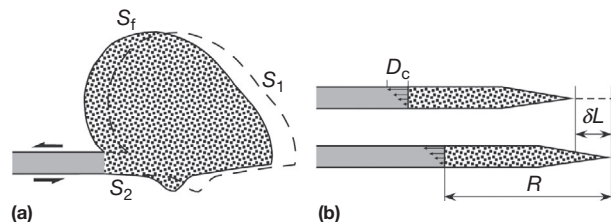


Figure 6 Schematic view of inelastic deformation associated with crack propagation. (a) Finite damage zone extending off the fault plane. (b) Thin in-plane damage zone.

result of which the crack acquires a new equilibrium configuration. In the new configuration, some area ahead of the crack front undergoes inelastic yielding and joins the process zone (see an area bounded by surfaces ΔS_1 and S_f in **Figure 6(a)**). At the trailing end of the process zone, slip exceeds D_c , and some fraction of the process zone (bounded by surface ΔS_2 in **Figure 6(a)**) joins the developed part of the crack. The external work δW is spent on changes in the elastic strain energy δU_e and irreversible inelastic deformation δU_G (which includes friction, breakdown, and comminution):

$$\delta W = \delta U_e + \delta U_G \quad [46]$$

Changes in the elastic strain energy are given by (e.g., Landau and Lifshitz, 1986; Timoshenko and Goodier, 1970)

$$\delta U_e = \frac{1}{2} \left(\sigma_{ij}^1 \epsilon_{ij}^1 - \sigma_{ij}^0 \epsilon_{ij}^0 \right) \quad [47]$$

where σ_{ij}^1 and ϵ_{ij}^1 are stresses and strains, respectively, in the elastic part of a medium after the crack extension. The assumption of linear elasticity [9] implies that

$$\sigma_{ij}^0 \epsilon_{ij}^1 \equiv \sigma_{ij}^1 \epsilon_{ij}^0 \quad [48]$$

for any σ_{ij}^k and ϵ_{ij}^k . The identity eqn [48] allows one to write eqn [47] as follows:

$$\delta U_e = \frac{1}{2} \left(\sigma_{ij}^1 + \sigma_{ij}^0 \right) \epsilon_{ij}^1 - \frac{1}{2} \left(\sigma_{ij}^1 + \sigma_{ij}^0 \right) \epsilon_{ij}^0 = \frac{1}{2} \left[\left(\sigma_{ij}^1 + \sigma_{ij}^0 \right) \delta u_i \right]_{,j} \quad [49]$$

where $\delta u_i = u_i^1 - u_i^0$ is the displacement field produced by crack propagation. Expressions [47] and [49] assume that the strains are infinitesimal, so that the relationship between strain and displacement gradients is given by eqn [8]. Also, expression [49] makes use of the fact that under quasistatic conditions, the divergence of stress is zero, $\sigma_{ij,j} = 0$ (see the equilibrium equations [10]; note that the body forces may be excluded from consideration by incorporating the effects of gravity in prestress). Using the Gauss theorem along with a condition that the crack-induced deformation must vanish at infinity, from the energy balance equation [46], one obtains the following expression for the work done on inelastic deformation:

$$\begin{aligned} \delta U_G &= \delta W - \delta U_e \\ &= - \int_{S_f} \sigma_{ij}^0 n_j \delta u_i dS - \frac{1}{2} \int_{\Delta S_1 + \Delta S_2} \left(\sigma_{ij}^0 + \sigma_{ij}^1 \right) n_j \delta u_i dS \quad [50] \end{aligned}$$

In the limit of an ideally brittle fracture, the area of inelastic yielding has a negligible volume (i.e., $S_f \rightarrow 0$), so that the first integral on the right-hand side of eqn [50] vanishes. In the second integral, the surface ΔS_2 also vanishes, while the surface ΔS_1 becomes the crack length increment δL (**Figure 6(b)**). Within δL , the stresses are weakly singular, $\sigma_{ij} \propto 1/\sqrt{r}$, where r is distance to the crack tip, and the crack wall displacements scale as $\delta u_i \propto \sqrt{r}$, so that the product of stresses and displacements is of the order of unity, and the corresponding integral in eqn [50] is of the order of $\Delta S_1 = \delta L$. This is the well-known LEFM limit, for which the fracture energy is given by eqn [2].

For more realistic models that explicitly consider failure at the crack tip, the stresses are finite everywhere, so that the

second integral on the right-hand side of eqn [50] is of the order of $\sigma_{ij}^0 \delta u_i (\Delta S_1 + \Delta S_2)$, that is, negligible compared to the integral over the finite inelastic zone $\sim O(\sigma_{ij}^0 \delta u_i S_f)$. Provided that the displacement field associated with the crack extension can be represented as $\delta u_i = \delta L \partial u_i / \partial L$, eqn [50] allows one to introduce the fracture energy G_c as the total inelastic work per increment of the crack length or the energy release rate:

$$G_c = \frac{\delta U_G}{\delta L} = -\frac{1}{2} \int_{S_f} \frac{\partial u_i}{\partial L} \sigma_{ij}^0 n_j dS \quad [51]$$

Factor of 1/2 in eqn [51] stems from the assumption of a bilateral crack propagation. Equation [51] in general cannot be readily evaluated analytically because the size and geometry of the inelastic zone S_f are not known in advance and have to be found as part of a solution. Further insights are possible for special cases. For example, assuming that all yielding is confined to a crack plane (**Figure 6(b)**), eqn [51] reduces to

$$G_c = \int_0^L \sigma(x) \frac{\partial D(x)}{\partial L} dx \quad [52]$$

where we took into account that the total offset between the crack walls is $D(x) = 2u_x$, and the sense of slip is opposite to that of the resisting shear tractions acting on the crack walls. The integral equation [52] is still intractable for an arbitrary loading, as the derivative $\partial D(x)/\partial L$ must be calculated along the equilibrium curve (e.g., see eqn [33]). Closed form analytic solutions can be obtained for limiting cases of small-scale ($L \gg R$) and large-scale ($L \approx R$) yielding. First, consider a crack that is much longer than the critical size L_c [36] and has a complete stress drop, $\sigma(x) = 0$ for $D > D_c$. As shown in **Section 4.03.2**, for such a crack the size of the process zone is independent of the crack length, $R = L_c$, and the crack propagation does not modify the slip distribution within the process zone in the reference frame of a propagating crack tip. In this case,

$$\partial D(x)/\partial L = -\partial D(x)/\partial x \quad [53]$$

so that eqn [52] gives rise to

$$G_c = \int_{L-R}^L \sigma(x) \frac{\partial D(x)}{\partial L} dx = \int_0^{D_c} \sigma(D) dD \quad [54]$$

Expression [54] is analogous to the result obtained using the J -integral technique (Rice, 1968b). An expression for the J -integral contains a derivative of the crack wall displacement with respect to the integration variable, rather than the crack length. As noted by Khazan and Fialko (2001), the two derivatives coincide (up to a sign) in a limiting case of a very long crack (for which the J -integral was derived), but the difference may be significant if the small-scale yielding approximation does not hold (also, see Rice, 1979).

For a case of a constant, but nonvanishing, residual friction, $\sigma(x) = \sigma_d$ for $D_c < D < D_m$, evaluation of integral equation [52] gives rise to

$$G_c = \sigma_d (D_m - D_c) + \int_0^{D_c} \sigma(D) dD \quad [55]$$

thanks to self-similarity of the along-crack displacement $D(x)$ over the interval $0 < x < L - R$ for long cracks, such that the

relationship [53] still holds. For a constant yield stress within the process zone, $\sigma(x) = \text{const} = \sigma_s$ (e.g., Figure 4), eqn [55] gives rise to a simple expression $G_c = (\sigma_s - \sigma_d)D_c + \sigma_d D_m$, in which the first and second terms may be recognized as the traditionally defined fracture energy U_G and the frictional work U_f , respectively (cf. eqn [45]).

In case of a large-scale yielding, relationship [53] is generally not applicable. Assuming $\sigma_s = \text{const}$, expression [52] can be integrated by parts to yield

$$G_c = \sigma_s \frac{\partial}{\partial L} \int_0^L D(x) dx - \sigma_s \int_0^F \frac{\partial D}{\partial L} dx \quad [56]$$

In the developed part of the crack with the full stress drop ($x < F$), slip is essentially constant and equals to D_c , so that the second integral on the right-hand side of eqn [56] can be neglected. Taking advantage of expressions [33] and [35] to evaluate the first term in eqn [56], one obtains (Khazan and Fialko, 2001)

$$G_c = \frac{\pi F}{2L_c} \sigma_s D_c \quad [57]$$

Equation [57] indicates that the fracture energy for the case of small cracks (or large-scale yielding, $F \ll L_c$) is substantially different from the fracture energy for large cracks (or small-scale yielding, $F \gg L_c$). In case of large-scale yielding, the fracture energy is not constant even if both the yield strength σ_s and the critical slip-weakening displacement D_c are material constants independent of loading conditions. In particular, G_c is predicted to linearly increase with the size of the developed part of the crack F . A linear scaling of fracture energy implies increases in the apparent fracture toughness K_{Ic} proportional to a square root of the developed crack length, $K_{Ic} \propto \sqrt{F}$ (see eqn [2]), in the large-scale yielding regime. Increases in the apparent fracture toughness for small cracks are well known from laboratory studies of tensile fracture (e.g., Bazant and Planas, 1998; Ingraffea and Schmidt, 1978).

The apparent scaling of the earthquake fracture energy with the earthquake size has been inferred from seismic data (e.g., Abercrombie and Rice, 2005; Hussein, 1977; Kanamori and Heaton, 2000). Arguments presented in the preceding text indicate that several mechanisms may be responsible for the observed increases in the seismically inferred fracture energies with the rupture length, in particular, (1) off-fault damage that scales with the rupture length (larger ruptures are expected to produce broader zones of high stress near the rupture fronts, presumably advancing the extent of off-fault damage (see Figure 5 and eqn [51])); (2) a continuous degradation of dynamic friction on a fault plane, for example, due to thermal pressurization or any other slip-weakening mechanism; and (3) rupture propagation under conditions of large-scale yielding (eqn [57]), although it remains to be seen whether elastodynamic instability can occur when the process zone comprises a substantial fraction of the crack length (see Section 4.03.4). These mechanisms are not mutually exclusive and may jointly contribute to the observed scaling $G_c \propto F$. For example, the third mechanism might be relevant for small earthquakes, while the first and second ones perhaps dominate for large events. Note that the second mechanism is ultimately limited by a complete stress drop, beyond which no further

increase in fracture energy is possible. The same limit may also apply to the first mechanism, as the size of the dynamic damage zone scales with the quasistatic one for a given displacement-weakening relationship (Rice et al., 2005). Establishing the relative importance of contributions of various mechanisms to the effective fracture energy is an important but challenging task. In particular, if contributions from the off-fault yielding are substantial, interpretations of seismic data that neglect such yielding may systematically overestimate the magnitude of the effective slip-weakening distance D_c . Unfortunately, distinguishing between different contributions to the overall value of G_c can be unlikely accomplished based on the seismic data alone.

In summary, the fracture energy defined by eqn [51] is analogous to Griffith's concept for tensile cracks, provided that the stress drop is complete ($\sigma_d = 0$) and the small-scale yielding condition is met. For a nonvanishing friction on the crack surface, eqn [51] combines inelastic work spent against residual friction and work spent on evolving the shear stress on a fault to a residual level (i.e., the traditionally defined fracture energy). Separation between these two contributions is justified if small-scale yielding condition applies but may be ill-defined otherwise. For models with a continuous strength degradation, there is a continuous repartitioning of the energy budget, such that the effective fracture energy increases at the expense of a diminishing frictional dissipation.

4.03.8 Coupling between Elastodynamics and Shear Heating

One of the factors that can strongly affect the dynamic friction on the slipping interface and, thereby, the seismic radiation, efficiency, and stress drop is the coseismic frictional heating. Rapid slip during seismic instabilities may substantially raise temperature on a fault surface. The dependence of dynamic friction on temperature may stem from several mechanisms, including thermal pressurization by pore fluids (Lachenbruch, 1980; Mase and Smith, 1987; Sibson, 1973), frictional melting (Jeffreys, 1942; Maddock, 1986; McKenzie and Brune, 1972; Sibson, 1975), and flash heating of contact asperities (Rice, 2006). Recent experimental measurements confirm appreciable variations in the dynamic friction at slip velocities approaching the seismic range of order of a meter per second (Brown and Fialko, 2012; Di Toro et al., 2004; Goldsby and Tullis, 2002, 2011; Hirose and Shimamoto, 2003; Reches and Lockner, 2010; Spray, 2005). The documented variations are significantly larger than predictions of the rate-and-state friction (Dieterich, 1979; Ruina, 1983) extrapolated to seismic slip rates. The likely importance of the thermally induced variations in friction warrants a quantitative insight into the dynamics of fault heating during seismic slip. Major questions include the following: What are the dominant mechanisms of fault friction at high slip rates? How do increases in temperature affect the dynamic shear stress on a slipping interface? How robust is the thermally activated weakening? Is dynamic friction a monotonically decaying function of temperature? If not, what are the mechanisms, conditions, and significance of the thermally activated strengthening? When and where is the onset of the thermally induced weakening or strengthening

likely to occur on a slipping interface? And what are the implications for the dynamics of earthquake ruptures?

In a simple case of the LEFM crack with a constant residual shear stress, the frictional heating problem admits closed analytic solutions (Fialko, 2004a; Richards, 1976). Consider a mode II (plain strain) crack rupturing bilaterally at a constant speed V_r (Figure 7), so that $L(t) = tV_r$. The thickness of the gouge layer that undergoes shear, and the shear strain rate across the gouge layer are assumed to be constant (Cardwell et al., 1978; Mair and Marone, 2000). Because the thickness of the gouge layer $2w$ is negligible compared with any other characteristic length scale in the problem (e.g., the rupture size $2L$ and the amount of slip D), the temperature evolution in the gouge layer and in the ambient rock is well described by the one-dimensional diffusion equation with a heat source:

$$\frac{\partial T}{\partial t} = \kappa \frac{\partial^2 T}{\partial y^2} + \frac{Q}{c\rho} \quad [58]$$

where y is the crack-perpendicular coordinate and Q is the rate of frictional heat generation within the slipping zone,

$$Q(x, y, t) = \begin{cases} \frac{\sigma_d(x)}{2w(x)} \frac{\partial D(x, t)}{\partial t}, & t > 0, |y| < w \\ 0, & |y| > w \end{cases} \quad [59]$$

$\partial D/\partial t$ being the local slip velocity. A solution to eqn [58] subject to the initial condition $T(x, y, 0) = T_0$, where T_0 is the temperature of the host rocks prior to faulting, is (Fialko, 2004a)

$$T - T_0 = \frac{1}{4c\rho w} \int_{x/V_r}^t \left(\operatorname{erf} \left[\frac{y+w}{2\sqrt{\kappa(t-\tau)}} \right] - \operatorname{erf} \left[\frac{y-w}{2\sqrt{\kappa(t-\tau)}} \right] \right) \frac{\partial D(x, \tau)}{\partial \tau} \sigma_d(x) d\tau \quad [60]$$

Dimensional arguments suggest the following similarity variables:

$$\text{Nondimensional along-fault coordinate } \chi = \frac{x}{tV_r} \quad [61]$$

$$\text{Nondimensional fault thickness } \bar{w} = \sqrt{\frac{2}{\kappa t}} w \quad [62]$$

For the LEFM crack with a constant stress drop, the along-crack displacement profile $D(x, t)$ is self-similar in that it may be expressed in terms of a single similarity variable $\chi = \chi(x, t)$:

$$D(x, t) = L(t)\epsilon\sqrt{1-\chi^2}, \quad t > 0, |\chi| < 1 \quad [63]$$

where ϵ is the characteristic shear strain due to the crack, $\epsilon = D(0, t)/L(t) = 2(1-\nu)(\sigma_0 - \sigma_d)/\mu$. Here, ϵ is taken to be independent of L , as the earthquake stress drops $(\sigma_0 - \sigma_d)$ do

not exhibit any scale dependence across a wide range of earthquake magnitudes (Abercrombie, 1995; Kanamori and Anderson, 1975; Scholz, 2002). The local slip rate in terms of new variables is

$$\frac{\partial D}{\partial t} = \frac{V_r \epsilon}{\sqrt{1-\chi^2}} \quad [64]$$

Equations [60] and [64] suggest the following similarity variable for temperature:

$$\text{Nondimensional temperature } \theta = \frac{T - T_0}{\hat{T}} \quad [65]$$

where

$$\hat{T} = \frac{\sigma_d V_r \epsilon}{c\rho} \sqrt{\frac{t}{\pi\kappa}} \quad [66]$$

is a characteristic temperature scale for frictional heating assuming a perfectly sharp fault contact.

Substituting eqn [64] into eqn [60] and making use of the similarity variables [62] and [65], one obtains the following expression for the along-crack temperature distribution in the middle of the slip zone ($y=0$):

$$\theta(\chi) = \frac{\sqrt{\pi}}{\bar{w}\sqrt{2}} \int_{\chi}^1 \operatorname{erf} \left[\frac{\bar{w}}{2\sqrt{2(1-\xi^2)}} \right] \frac{\xi d\xi}{\sqrt{\xi^2 - \chi^2}} \quad [67]$$

Solutions to eqn [67] are shown in Figure 8. A family of curves in Figure 8 illustrates a spatiotemporal evolution of temperature on the slipping fault surface. For faults that are

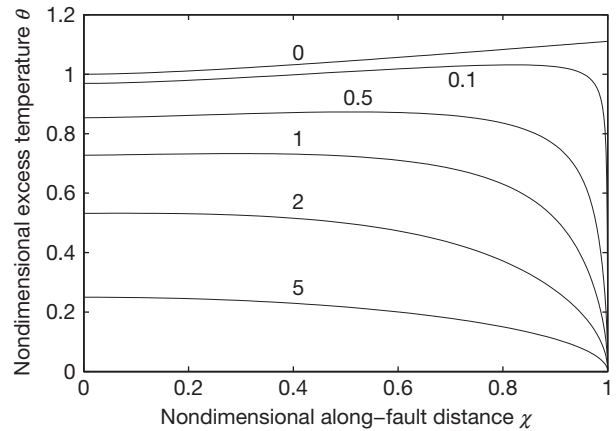


Figure 8 Variations of the nondimensional excess temperature $\theta(\chi)$ along a mode II crack propagating at a constant rupture speed under constant frictional stress. Labels denote the nondimensional thickness of a slipping zone \bar{w} (see eqn [62]).

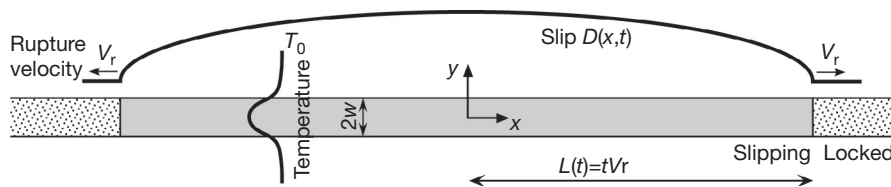


Figure 7 A schematic view of a dynamically propagating mode II crack. The crack has a thickness $2w$ and is rupturing bilaterally at a constant velocity $dL/dt = V_r$.

thicker than the thermal diffusion length scale or at early stages of rupture (i.e., $\bar{w} > 1$), the temperature increase along the fault is proportional to the amount of slip. For thin faults or later during the rupture ($\bar{w} \ll 1$), the temperature is maximum near the crack tip and decreases from the tip to the crack center. However, the instantaneous temperature maximum near the crack tip does not imply cooling of the crack surface behind the tip; at any given point, the temperature on the crack surface $T(x, 0, t)$ steadily increases with time (Fialko, 2004a). For the nondimensional fault thickness \bar{w} of the order of unity, the maximum temperature is reached somewhere between the crack center and the rupture front (Figure 8). The inferred anticorrelation between the temperature and the amount of slip stems from a competition between the rates at which the frictional heat is generated at the crack surface and removed to the ambient rocks by conduction. Generation of frictional heat at the tip of the LEFM crack is singular as the thickness of the conductive boundary layer is zero, while the slip velocity is infinite (see eqn [64]). Nonetheless, the excess temperature at the tip is zero for cracks having finite thickness ($\bar{w} > 0$). For cracks that are much thinner than the conductive boundary layer ($\bar{w} \ll 1$), the temperature field develops a shock-like structure, with the tip temperature exceeding the temperature at the crack center by about 10% (Figure 8). Assuming that the thickness of the slip zone is constant during an earthquake, eqn [67] predicts that the maximum temperatures are initially attained at the center of a cracklike shear instability. As the earthquake rupture expands, the temperature maximum may migrate toward the rupture fronts. For the thermal diffusivity of the ambient rocks $\kappa = 10^{-6} \text{ m}^2 \text{ s}^{-1}$ and rupture durations of $t = 1\text{--}10 \text{ s}$ (corresponding to the rupture sizes of $\sim 5\text{--}50 \text{ km}$), this transition will occur for faults that have thickness of the order of $\sqrt{2\kappa t} \sim 2\text{--}5 \text{ mm}$ or less. The critical fault thickness may be larger still if the heat removal from the fault involves some advective transport by the pressurized pore fluids, and the *in situ* hydraulic diffusivity exceeds the thermal diffusivity κ .

For sufficiently large ruptures, a model of a self-healing slip pulse may be a better approximation than the cracklike models (e.g., Beroza and Mikumo, 1996; Heaton, 1990; Kanamori and Anderson, 1975; Olsen et al., 1997). A self-healing mode II pulse having a constant length L (Freund, 1979) generates a temperature field that is steady state in the reference frame of a moving rupture front (Fialko, 2004a). The appropriate similarity variables are

$$\text{along-fault coordinate } \chi = \frac{x - tV_r}{L} + 1 \quad [68]$$

$$\text{nondimensional fault thickness } \bar{w} = \sqrt{\frac{2V_r}{L\kappa}} w \quad [69]$$

$$\text{nondimensional temperature } \theta = \frac{T - T_0}{\hat{T}} \quad [70]$$

$$\hat{T} = \frac{\sigma_d \epsilon}{c\rho} \sqrt{\frac{LV_r}{\pi\kappa}} \quad [71]$$

The coseismic displacements and the rate of slip are assumed to have the LEFM-like characteristics at the rupture front ($\chi = 1$) and a nonsingular healing at the trailing edge ($\chi = 0$):

$$D(\chi) = L\epsilon\sqrt{1-\chi^2} \quad [72]$$

$$\frac{\partial D}{\partial \chi} = \frac{V_r \epsilon \chi}{\sqrt{1-\chi^2}} \quad [73]$$

As before, we assume a constant dynamic friction on the slipping interface. Upon nondimensionalization using variables [71], eqn [60] gives rise to the following expression for the along-fault temperature variations in the middle of the slip zone ($y = 0$):

$$\theta(\chi) = \frac{\sqrt{\pi}}{\bar{w}\sqrt{2}} \int_{\chi}^1 \text{erf} \left[\frac{\bar{w}}{2\sqrt{2}(\chi-\xi)} \right] \frac{\xi d\xi}{\sqrt{1-\xi^2}} \quad [74]$$

Solutions to eqn [74] are shown in Figure 9. The near-tip structure of the temperature field due to a steady-state pulse is similar to that due to a self-similar expanding crack (cf. Figures 8 and 9). At the leading edge of an infinitesimally thin shear pulse, there is a thermal shock of amplitude \hat{T} (eqn [71]). The fault temperature monotonically decreases toward the healing front, where the temperature falls to about one-half of the maximum value (Figure 9). For 'thick' pulses ($\bar{w} \gg 1$), the fault temperature increases toward the healing front proportionally to the amount of slip. For intermediate nondimensional fault thicknesses of the order of unity, the fault surface initially heats up to a maximum temperature and then cools down before the arrival of the healing front. This behavior is qualitatively different from that on a surface of an expanding crack, which indicates a progressive heating at every point along the crack as long as the rupture continues. The inferred cooling toward the healing front of the steady-state pulse for $\bar{w} > 5$ is caused by a decreasing heat generation due to a vanishing slip velocity and efficient removal of heat by thermal diffusion. For the characteristic rise times L/V_r of the order of seconds, the steady-state LEFM pulses need to be thinner than $5\sqrt{2\kappa L/V_r} \approx 1 \text{ cm}$ to experience maximum temperatures at the rupture front.

Several factors may accentuate the tendency for the temperature peaks near the rupture front. First, higher stresses in the process zone near the rupture tip imply enhanced heating. Numerical simulations indicate that the thermal effect of the

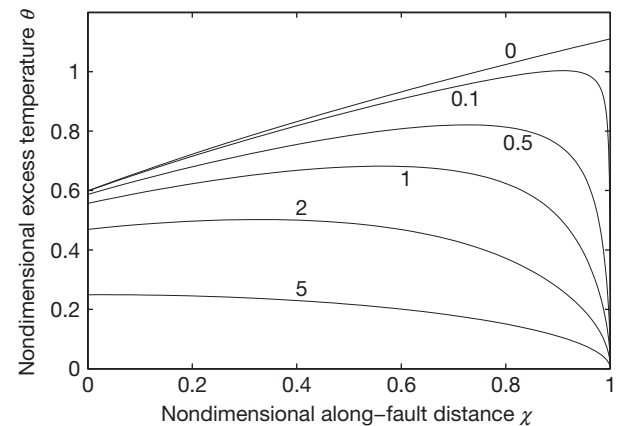


Figure 9 Variations of the nondimensional excess temperature $\theta(\chi)$ along a self-healing pulse. Labels denote the nondimensional thickness of a slipping zone w (see eqns [71]).

process zone can be significant even under conditions of small-scale yielding; in particular, for thin faults, the instantaneous temperature increase within the process zone is predicted to be a factor of σ_s/σ_d greater than the temperature increase on the rest of the slipping interface (Fialko, 2004a). Second, in the presence of a continued dynamic weakening (e.g., Abercrombie and Rice, 2005), the frictional heating is expected to progressively decay behind the rupture front, further suppressing the excess temperature. In the context of thermal weakening, such coupling between the coseismic heating and dynamic friction may be conducive to self-sustained slip pulses (Noda et al., 2009; Perrin et al., 1995; Zheng and Rice, 1998) and to a transition to a pulse-like behavior for ruptures that initially propagate in a cracklike mode.

Numerical simulations that allow for full coupling between the shear stress, shear heating, pore fluid pressure, and elasticity indicate a rich variety of slip behaviors and important controls exerted by the effective thickness of the fault slip zone w . For example, Garagash (2012) showed that in the presence of thermal pressurization, spontaneous fault slip can occur in the form of slip pulses, with the rupture speed V_r inversely correlated with the thickness of the slip zone. For the laboratory values of hydraulic and thermal properties of fault gouge, the model predicts earthquake-like behavior for slip zones having thickness of the order of centimeters (or thinner), an aseismic episodic slip with characteristics similar to those of the episodic slow slip events observed in subduction zones worldwide (Obara, 2002; Rogers and Dragert, 2003), assuming width of the slip zone of the order of 1 m (Garagash, 2012).

If thermal weakening mechanisms that operate at relatively small increases in the average fault temperature, such as thermal pressurization and flash melting (e.g., Andrews, 2002; Goldsby and Tullis, 2011; Lachenbruch, 1980; Lee and Delaney, 1987; Rice, 2006), do not give rise to substantial reductions in the dynamic friction, a continued dissipation and heating due to a localized slip will result in macroscopic melting on the slip interface and a transition from the asperity-contact friction to viscous rheology. High transient stresses associated with shearing of thin viscous films of melt have been considered as one of possible mechanisms of thermally induced strengthening (Fialko, 2004a; Koizumi et al., 2004; Tsutsumi and Shimamoto, 1997). However, recent laboratory, field, and theoretical studies suggest that transient viscous braking may not be an efficient arresting mechanism, especially in the lower part of the brittle layer (Brown and Fialko, 2012; Di Toro et al., 2006; Fialko and Khazan, 2005). If so, earthquakes that produced macroscopic melting and pseudotachylites (e.g., Davidson et al., 2003; Sibson, 1975; Swanson, 1992; Wenk et al., 2000) must have been accompanied by nearly complete stress drops. More generally, one may argue that highly localized slip zones are an indicator of nearly complete stress drops for sizeable earthquakes, regardless of whether macroscopic melting took place. This stems from the fact that melting of a narrow slip interface could have been prevented only if the dynamic friction were already low (Fialko, 2004a). Some theoretical arguments and experimental data (Brown and Fialko, 2012; Di Toro et al., 2006; Fialko and Khazan, 2005; Mitchell et al., 2013) also raise a question about the mechanism of rupture arrest below the brittle-ductile

transition. A currently prevailing view is that the bottom of the seismogenic layer represents a rheological transition between the velocity-weakening friction and velocity-strengthening friction (e.g., Marone, 1998; Scholz, 1998). While this transition may well be caused by the temperature-controlled onset of stable creep (although recent laboratory data revealed a possibility of stick-slip behavior in granite at temperatures well above 300 °C, at least under dry conditions; see, e.g., Mitchell et al., 2013), it is unclear whether the velocity strengthening is relevant for the arrest of seismic ruptures that propagate into the ductile substrate from the brittle upper crust. For highly localized ruptures, the onset of melting or some other thermally activated mechanism may occur immediately behind the rupture front (aided by high ambient temperature and stress concentration), potentially overwhelming the effect of rate-and-state friction. In this case, the rupture arrest may require either delocalization of seismic slip near the rupture front (thereby limiting the temperature rise and increasing the effective fracture energy) or low deviatoric stress below the brittle-ductile transition. Discriminating between these possibilities may provide important insights into long-standing questions about the effective mechanical thickness and strength of tectonically active crust and lithosphere (England and Molnar, 1997; Jackson, 2002; Lamb, 2002; Takeuchi and Fialko, 2012).

4.03.9 Conclusions

Shear tractions on a slipping fault may be controlled by a multitude of physical processes that include yielding and breakdown around the propagating rupture front, rate- and slip-dependent friction, acoustic fluidization, dynamic reduction in the fault-normal stress due to dissimilar rigidities of the fault walls, thermally activated increases in the pore fluid pressure, flash heating of the asperities, and macroscopic melting. A traditional distinction between the fracture energy consumed near the rupture front and frictional losses on a well-slipped portion of a fault may be ill-defined if the slipping interface undergoes a substantial yet gradual weakening behind the rupture front. Both theoretical models and experimental data indicate that a continuous degradation of the dynamic fault strength is an expected consequence of a highly localized slip. In this case, earthquake ruptures violate a basic assumption of the LEFM, namely, that the zone of the material breakdown is small compared to the rupture size. The assumption of small-scale yielding is also violated if the extent of the off-fault damage is not negligible compared to the characteristic length of a slipping region. Field observations of kilometer-wide damage zones around major crustal faults (Ambraseys, 1970; Chen and Freymueller, 2002; Fialko, 2004b; Fialko et al., 2002) are evidence that the off-fault yielding may constitute a significant fraction of the earthquake energy balance (Wilson et al., 2004).

Both the dynamically induced variations in shear stress along the slip interface and distributed inelastic deformation off the primary slip surface affect the distribution of slip and slip rate, dynamic stress drop, and radiated seismic energy. Inferences from seismic data about constitutive properties of the fault zone material, such as the peak breakdown stress and critical slip-weakening distance, may be biased if the

aforementioned phenomena are not taken into account. In particular, simplified rupture models that neglect off-fault damage likely overestimate the critical slip-weakening distance D_c . Similarly, models that neglect the physics of high-speed slip may attribute the dynamic (e.g., thermally induced) weakening to large *in situ* values of D_c interpreted as an intrinsic rock fracture property. Constitutive relationships governing evolution of the dynamic strength at seismic slip velocities are difficult to formalize, as temperature, pore fluid pressure, and shear tractions on the fault interface are sensitive to a number of parameters such as the effective thickness of the slip zone, fluid saturation, dynamic damage and changes in the fault wall permeability, and ambient stress. Many of these parameters are also poorly constrained by the available data. Nonetheless, further insights into the dynamics of earthquakes may require fully coupled elastodynamic–thermodynamic models of seismic rupture. Development of such models is a significant challenge for future work.

Acknowledgments

I thank Jim Rice, Allan Rubin, and Hiroo Kanamori for their insightful reviews. Jim Rice kindly provided results of his calculations of off-fault damage (Figure 5). This work was supported by NSF through grants EAR-0338061, EAR-0450035, and EAR-0944336.

References

- Abercrombie R (1995) Earthquake source scaling relationships from -1 to $5 M_w$ using seismograms recorded at 2.5-km depth. *Journal of Geophysical Research* 100: 24015–24036.
- Abercrombie R and Rice JR (2005) Can observations of earthquake scaling constrain slip weakening? *Geophysical Journal International* 162: 406–424.
- Aki K (1967) Scaling law of seismic spectrum. *Journal of Geophysical Research* 72: 1217–1231.
- Aki K and Richards PG (1980) *Quantitative Seismology: Theory and Methods, I and II*, p. 577. San Francisco, CA: W. H. Freeman.
- Ambraseys N (1970) Some characteristic features of the North Anatolian fault zone. *Tectonophysics* 9: 143–165.
- Ampuero J and Rubin AM (2008) Earthquake nucleation on rate and state faults – Aging and slip laws. *Journal of Geophysical Research* 113: B01302.
- Andrews DJ (1976a) Rupture propagation with finite stress in antiplane strain. *Journal of Geophysical Research* 81: 3575–3582.
- Andrews DJ (1976b) Rupture velocity of plane strain shear cracks. *Journal of Geophysical Research* 81: 5679–5687.
- Andrews DJ (2002) A fault constitutive relation accounting for thermal pressurization of pore fluid. *Journal of Geophysical Research* 107: ESE 15–1–ESE 15–8. <http://dx.doi.org/10.1029/2002JB001942>.
- Andrews DJ (2005) Rupture dynamics with energy loss outside the slip zone. *Journal of Geophysical Research* 110: B01307. <http://dx.doi.org/10.1029/2004JB003191>.
- Aochi H and Madariaga R (2003) The 1999 Izmit, Turkey, earthquake: Nonplanar fault structure, dynamic rupture process, and strong ground motion. *Bulletin of the Seismological Society of America* 93: 1249–1266.
- Archuleta RJ (1984) A faulting model for the 1979 Imperial Valley earthquake. *Journal of Geophysical Research* 89: 4559–4585.
- Atkinson BK (1987) Introduction to fracture mechanics. In: Atkinson BK (ed.) *Fracture Mechanics of Rock*, pp. 1–23. London: Academic Press, chapter 1.
- Barenblatt GI (1959) The formation of equilibrium cracks during brittle fracture. General ideas and hypotheses. Axially-symmetric cracks. *Journal of Applied Mathematics and Mechanics* 23: 622–636 (in Russian).
- Barton N (1971) A relationship between joint roughness and joint shear strength. In: *Proceedings of International Symposium on Rock Mechanics, Nancy, Pap. I-8*.
- Bazant ZP and Planas J (1998) *Fracture and Size Effect in Concrete and Other Quasibrittle Materials*. Boca Raton, FL: CRC Press.
- Ben-Zion Y (2003) Appendix 2, key formulas in earthquake seismology. In: Lee W, Kanamori H, Jennings P, and Kisslinger C (eds.) *International Handbook of Earthquake and Engineering Seismology*, Vol. 81B, pp. 1857–1875. Amsterdam: Academic Press.
- Ben-Zion Y and Rice JR (1997) Dynamic simulations of slip on a smooth fault in an elastic solid. *Journal of Geophysical Research* 102: 17771–17784.
- Ben-Zion Y and Shi Z (2005) Dynamic rupture on a material interface with spontaneous generation of plastic strain in the bulk. *Earth and Planetary Science Letters* 236: 486–496.
- Beroza GC and Mikumo T (1996) Short slip duration in dynamic rupture in the presence of heterogeneous fault properties. *Journal of Geophysical Research* 101: 22449–22460.
- Beroza GC and Spudich P (1988) Linearized inversion for fault rupture. *Journal of Geophysical Research* 93: 6275–6296.
- Bilby BA and Eshelby JD (1968) Dislocations and the theory of fracture. In: Liebowitz H (ed.) *Fracture: An Advanced Treatise*, vol. 1, pp. 99–182. New York: Academic Press.
- Blanpied M, Tullis T, and Weeks J (1995) Frictional slip of granite at hydrothermal conditions. *Journal of Geophysical Research* 100: 13045–13064.
- Bouchon M and Vallee M (2003) Observation of long supershear rupture during the magnitude 8.1 Kunlunshan earthquake. *Science* 301: 824–826.
- Broberg K (1978) Transient sliding motion. *Geophysical Journal of the Royal Astronomical Society* 52: 397–432.
- Broberg K (1987) On crack paths. *Engineering Fracture Mechanics* 28: 663–679.
- Broberg K (1989) The near-tip field at high crack velocities. *International Journal of Fracture* 39: 1–13.
- Broberg K (1999) *Cracks and Fracture*. London: Academic Press.
- Brodsky EE and Kanamori H (2001) Elastohydrodynamic lubrication of faults. *Journal of Geophysical Research* 106: 16357–16374.
- Brown KM and Fialko Y (2012) “Melt well” mechanism of extreme weakening of gabbro at seismic slip rates. *Nature* 488: 638–641.
- Brune JN, Henyey T, and Roy R (1969) Heat flow, stress, and rate of slip along San Andreas fault, California. *Journal of Geophysical Research* 74: 3821–4009.
- Brune J and Thatcher W (2002) Strength and energetics of active fault zones. In: Lee W, Kanamori H, Jennings P, and Kisslinger C (eds.) *International Handbook of Earthquake and Engineering Seismology*, Vol. 81B, pp. 569–588. Amsterdam: Academic Press.
- Burridge R (1973) Admissible speeds for plane-strain self-similar shear cracks with friction but lacking cohesion. *Geophysical Journal of the Royal Astronomical Society* 35: 439–455.
- Burridge R and Holliday G (1971) Dynamic shear cracks with friction as models for shallow focus earthquakes. *Geophysical Journal of the Royal Astronomical Society* 25: 261–283.
- Byerlee J (1978) Friction of rock. *Pure and Applied Geophysics* 116: 615–626.
- Cardwell R, Chinn D, Moore G, and Turcotte D (1978) Frictional heating on a fault zone with finite thickness. *Geophysical Journal of the Royal Astronomical Society* 52: 525–530.
- Chen Q and Freymueller J (2002) Geodetic evidence for a near-fault compliant zone along the San Andreas fault in the San Francisco Bay area. *Bulletin of the Seismological Society of America* 92: 656–671.
- Chen YT and Knopoff L (1986) Static shear crack with a zone of slip-weakening. *Geophysical Journal of the Royal Astronomical Society* 87: 1005–1024.
- Cherepanov GP (1968) Cracks in solids. *International Journal of Solids and Structures* 4: 811–831.
- Cherepanov GP (1979) *Mechanics of Brittle Fracture*. Berlin, Heidelberg: Springer Verlag.
- Chester JS, Chester FM, and Kronenberg AK (2005) Fracture surface energy of the Punchbowl fault, San Andreas system. *Nature* 437: 133–136.
- Cowie PA and Scholz CH (1992) Physical explanation for the displacement–length relationship of faults using a post-yield fracture mechanics model. *Journal of Structural Geology* 14: 1133–1148.
- Dahlen FA (1977) The balance of energy in earthquake faulting. *Geophysical Journal of the Royal Astronomical Society* 48: 239–261.
- Dahlen FA and Tromp J (1998) *Theoretical Global Seismology*, p. 944. Princeton, NJ: Princeton University Press.
- Davidson C, Davis K, Bailey C, Tape C, Singleton J, and Singer B (2003) Age, origin, and significance of brittle faulting and pseudotachylite along the coast shear zone, prince rupert, British Columbia. *Geology* 31: 43–46.
- Day SM (1982) Three-dimensional simulation of spontaneous rupture: The effect of nonuniform prestress. *Bulletin of the Seismological Society of America* 72: 1881–1902.

- Delouis B, Giardini D, Lundgren P, and Salichon J (2002) Joint inversion of InSAR, GPS, teleseismic, and strong-motion data for the spatial and temporal distribution of earthquake slip: Application to the 1999 Izmit mainshock. *Bulletin of the Seismological Society of America* 92: 278–299.
- Di Toro G, Goldsby DL, and Tullis TE (2004) Friction falls towards zero in quartz rock as slip velocity approaches seismic rates. *Nature* 427: 436–439.
- Di Toro G, Hirose T, Nielsen S, Pennacchioni G, and Shimamoto T (2006) Natural and experimental evidence of melt lubrication of faults during earthquakes. *Science* 311: 647–649.
- Dieterich JH (1979) Modeling of rock friction 1. Experimental results and constitutive equations. *Journal of Geophysical Research* 84: 2161–2168.
- Dieterich JH (1992) Earthquake nucleation on faults with rate- and state-dependent strength. *Tectonophysics* 211: 115–134.
- Dugdale DS (1960) Yielding of steel sheets containing slits. *Journal of the Mechanics and Physics of Solids* 8: 100–115.
- Dunham EM and Archuleta RJ (2004) Evidence for a supershear transient during the 2002 Denali fault earthquake. *Bulletin of the Seismological Society of America* 94: S256–S268.
- England PC and Molnar P (1997) Active deformation of Asia: From kinematics to dynamics. *Science* 278: 647–650.
- Eshelby JD (1956) The continuum theory of lattice defects. In: Seitz F and Turnbull D (eds.) *Progress in Solid State Physics*, pp. 79–144. New York: Academic Press.
- Fialko Y (2004a) Temperature fields generated by the elastodynamic propagation of shear cracks in the Earth. *Journal of Geophysical Research* 109: B01303. <http://dx.doi.org/10.1029/2003JB002497>.
- Fialko Y (2004b) Probing the mechanical properties of seismically active crust with space geodesy: Study of the co-seismic deformation due to the 1992 M_w 7.3 Landers (southern California) earthquake. *Journal of Geophysical Research* 109: B03307. <http://dx.doi.org/10.1029/2003JB002756>.
- Fialko Y and Khazan Y (2005) Fusion by earthquake fault friction: Stick or slip? *Journal of Geophysical Research* 110: B12407. <http://dx.doi.org/10.1029/2005JB003869>.
- Fialko Y, Rivera L, and Kanamori H (2005) Estimate of differential stress in the upper crust from variations in topography and strike along the San Andreas fault. *Geophysical Journal International* 160: 527–532.
- Fialko YA and Rubin AM (1997) Numerical simulation of high pressure rock tensile fracture experiments: Evidence of an increase in fracture energy with pressure? *Journal of Geophysical Research* 102: 5231–5242.
- Fialko Y, Sandwell D, Agnew D, Simons M, Shearer P, and Minster B (2002) Deformation on nearby faults induced by the 1999 Hector Mine earthquake. *Science* 297: 1858–1862.
- Freund LB (1979) The mechanics of dynamic shear-crack propagation. *Journal of Geophysical Research* 84: 2199–2209.
- Freund LB (1998) *Dynamic Fracture Mechanics*, p. 563. New York: Cambridge University Press.
- Gakhov FD (1966) *Boundary Value Problems*. London: Pergamon Press.
- Garagash D (2012) Seismic and aseismic slip pulses driven by thermal pressurization of pore fluid. *Journal of Geophysical Research* 117: B04314.
- Goldsby D and Tullis T (2002) Low frictional strength of quartz rocks at subseismic slip rates. *Geophysical Research Letters* 29: 25–1–25–4. <http://dx.doi.org/10.1029/2002GL015240>.
- Goldsby D and Tullis T (2011) Flash heating leads to low frictional strength of crustal rocks at earthquake slip rates. *Science* 334: 216–218.
- Griffith AA (1920) The phenomena of rupture and flow in solids. *Philosophical Transactions of the Royal Society of London A* 221: 163–197.
- Gu J-C, Rice JR, Ruina AL, and Tse ST (1984) Slip motion and stability of a single degree of freedom elastic system with rate and state dependent friction. *Journal of the Mechanics and Physics of Solids* 32: 167–196.
- Gutenberg B and Richter C (1949) *Seismicity of the Earth and Associated Phenomena*. Princeton: Princeton University Press.
- Hartzell SH and Heaton T (1983) Inversion of strong ground motion and teleseismic waveform data for the fault rupture history of the 1979 Imperial Valley, California, earthquake. *Bulletin of the Seismological Society of America* 73: 1553–1583.
- Hashida T, Oghikubo H, Takahashi H, and Shoji T (1993) Numerical simulation with experimental-verification of the fracture-behavior in granite under confining pressures based on the tension-softening model. *International Journal of Fracture* 59: 227–244.
- Heaton T (1990) Evidence for and implications of self-healing pulses of slip in earthquake rupture. *Physics of the Earth and Planetary Interiors* 64: 1–20.
- Hirose T and Shimamoto T (2003) Fractal dimension of molten surfaces as a possible parameter to infer the slip-weakening distance of faults from natural pseudotachylytes. *Journal of Structural Geology* 25: 1569–1574.
- Hirose T and Shimamoto T (2005) Growth of molten zone as a mechanism of slip weakening of simulated faults in gabbro during frictional melting. *Journal of Geophysical Research* 110: B05202. <http://dx.doi.org/10.1029/2004JB003207>.
- Hussein MI (1977) Energy balance for formation along a fault. *Geophysical Journal of the Royal Astronomical Society* 49: 699–714.
- Ida Y (1972) Cohesive force across the tip of a longitudinal-shear crack and Griffith's specific surface energy. *Journal of Geophysical Research* 77: 3796–3805.
- Inglis CE (1913) Stresses in a plate due to the presence of cracks and sharp corners. *Transactions of the Royal Institution of Naval Architects* 55: 219–241.
- Ingraffea AR and Schmidt RA (1978) Experimental verification of a fracture mechanics model for tensile strength prediction of Indiana limestone. In: Kim Y-S (ed.) *Proceedings of the 19th US Symposium on Rock Mechanics*, pp. 247–253. Reno: University of Nevada.
- Irwin GR (1957) Relation of stresses near a crack to the crack extension force. In: *Proceedings of 9th International Congress on Applied Mechanics, Vol. VIII*, pp. 245–251.
- Jackson J (2002) Strength of the continental lithosphere: Time to abandon the jelly sandwich? *GSA Today* 12: 4–9.
- Jeffreys H (1942) On the mechanics of faulting. *Geological Magazine* 79: 291–295.
- Kame N and Yamashita T (1999) Simulation of the spontaneous growth of a dynamic crack without constraints on the crack tip path. *Geophysical Journal International* 139: 345–358.
- Kanamori H (2004) The diversity of the physics of earthquakes. *Proceedings of the Japan Academy, Series B* 80: 297–316.
- Kanamori H and Anderson DL (1975) Theoretical basis of some empirical relations in seismology. *Bulletin of the Seismological Society of America* 65: 1073–1095.
- Kanamori H and Brodsky EE (2004) The physics of earthquakes. *Reports on Progress in Physics* 67: 1429–1496.
- Kanamori H and Heaton TH (2000) Microscopic and macroscopic physics of earthquakes. In: Rundle J, Turcotte DL, and Klein W (eds.) *Physics of Earthquakes. Geophysical Monograph*, vol. 106, pp. 117–136. Washington, DC: AGU.
- Khazan YM and Fialko YA (1995) Fracture criteria at the tip of fluid driven cracks in the Earth. *Geophysical Research Letters* 22: 2541–2544.
- Khazan YM and Fialko Y (2001) Tensile and shear cracks in the Dugdale–Barenblatt model. *Geofizicheskiy Zhurnal* 23: 13–30 (in Russian).
- Koizumi YK, Otsuki TA, and Nagahama H (2004) Frictional melting can terminate seismic slips: Experimental results of stick-slips. *Geophysical Research Letters* 31. <http://dx.doi.org/10.1029/2004GL020642>, Art. No. L21,605.
- Kolosoff GV (1909) *On an Application of Complex Function Theory to a Plane Problem of the Mathematical Theory of Elasticity*. Yuriev.
- Kostrov BV (1970) Tectonic earthquake focal theory. *Izvestiya Akademii Nauk SSSR, Earth Physics* 4: 84–101.
- Kostrov BV (1974) Seismic moment and energy of earthquakes and seismic flow of rock. *Izvestiya, Academy of Sciences, USSR, Physics of the Solid Earth (Engl. Translation)* 1: 23–40.
- Kostrov BV and Das S (1988) *Principles of Earthquake Source Dynamics*, p. 286. Cambridge: Cambridge University Press.
- Lachenbruch AH (1980) Frictional heating, fluid pressure, and the resistance to fault motion. *Journal of Geophysical Research* 85: 6097–6112.
- Lamb S (2002) Is it all in the crust? *Nature* 420: 130–131.
- Landau LD and Lifshitz EM (1986) *Theory of Elasticity*, p. 187. Oxford: Pergamon Press.
- Lapusta N and Rice JR (2004) Earthquake sequences on rate and state faults with strong dynamic weakening. *EOS, Transactions, American Geophysical Union, Supplement* 84: S51B02.
- Law N (1993) *Fracture of Brittle Solids*, 2nd edn, p. 378. Cambridge: Cambridge University Press.
- Lee T-C and Delaney P (1987) Frictional heating and pore pressure rise due to fault slip. *Geophysical Journal of the Royal Astronomical Society* 88: 569–591.
- Leonov MY and Panasyuk VV (1959) The development of very small cracks in a solid. *Zhurnal Prikladnoi Mekhaniki i Tekhnicheskoi Fiziki (Applied Mechanics)* 5: 391–401 (in Ukrainian).
- Li VC (1987) Mechanics of shear rupture applied to earthquake zones. In: Atkinson B (ed.) *Fracture Mechanics of Rock*, pp. 351–428. London: Academic Press.
- Li Y, Aki K, Vidale J, and Alvarez M (1998) A delineation of the Nojima fault ruptured in the M7.2 Kobe, Japan, earthquake of 1995 using fault zone trapped waves. *Journal of Geophysical Research* 103(B4): 7247–7263.
- Lockner DA, Byerlee J, Kukusenko V, Ponomarev A, and Sidorin A (1992) Observations of quasistatic fault growth from acoustic emissions. In: Evans B and Wong T (eds.) *Fault Mechanics and Transport Properties of Rocks*, pp. 3–31. San Diego, CA: Academic.
- Madariaga R (1976) Dynamics of an expanding circular fault. *Bulletin of the Seismological Society of America* 66: 636–666.
- Maddock R (1986) Frictional melting in landslide-generated frictionites (hyalomylonites) and fault-generated pseudotachylytes – Discussion. *Tectonophysics* 128: 151–153.
- Mair K and Marone C (2000) Shear heating in granular layers. *Pure and Applied Geophysics* 157: 1847–1866.

- Malvern LE (1969) *Introduction to the Mechanics of a Continuum Medium*, p. 713. Englewood Cliffs, NJ: Prentice-Hall.
- Manighetti I, King G, Gaudemer Y, Scholz C, and Doubre C (2001) Slip accumulation and lateral propagation of active normal faults in Afar. *Journal of Geophysical Research* 106: 13667–13696.
- Marone C (1998) Laboratory-derived friction laws and their application to seismic faulting. *Annual Review of Earth and Planetary Sciences* 26: 643–696.
- Mase CW and Smith L (1987) Effects of frictional heating on the thermal, hydrologic, and mechanical response of a fault. *Journal of Geophysical Research* 92: 6249–6272.
- McKenzie D and Brune JN (1972) Melting on fault planes during large earthquakes. *Geophysical Journal of the Royal Astronomical Society* 29: 65–78.
- Melin S (1986) When does a crack grow under mode II conditions. *International Journal of Fracture* 30: 103–114.
- Mitchell E, Fialko Y, and Brown KM (2013) Temperature dependence of frictional healing of Westerly granite: Experimental observations and numerical simulations. *Geochemistry, Geophysics, Geosystems* 14: 567–582.
- Molinari A, Estrin Y, and Mercier S (1999) Dependence of the coefficient of friction on the sliding conditions in the high velocity range. *Journal of Tribology* 121: 35–41.
- Muskhelishvili NI (1953) *Some Basic Problems of Mathematical Theory of Elasticity*. Groningen, Holland: Noordhoff.
- Noda H, Dunham E, and Rice JR (2009) Earthquake ruptures with thermal weakening and the operation of major faults at low overall stress levels. *Journal of Geophysical Research* 114: B07,302.
- Obara K (2002) Nonvolcanic deep tremor associated with subduction in southwest Japan. *Science* 296: 1679.
- Oglesby DD and Archuleta RJ (2001) Fault geometry and the dynamics of the 1999 Chi-Chi (Taiwan) earthquake. *Bulletin of the Seismological Society of America* 91: 1099–1111.
- Ohnaka M (2003) A constitutive scaling law and a unified comprehension for frictional slip failure, shear fracture of intact rock, and earthquake rupture. *Journal of Geophysical Research* 108: B2080. <http://dx.doi.org/10.1029/2000JB000123>.
- Okada Y (1985) Surface deformation due to shear and tensile faults in a half-space. *Bulletin of the Seismological Society of America* 75: 1135–1154.
- Olsen K, Madariaga R, and Archuleta R (1997) Three-dimensional dynamic simulation of the 1992 Landers earthquake. *Science* 278: 834–838.
- Palmer AC and Rice JR (1973) The growth of slip surfaces in the progressive failure of over-consolidated clay. *Proceedings of the Royal Society of London, Series A* 332: 527–548.
- Perrin G, Rice JR, and Zheng G (1995) Self-healing slip pulse on a frictional surface. *Journal of the Mechanics and Physics of Solids* 43: 1461–1495.
- Peyrat S, Olsen K, and Madariaga R (2001) Dynamic modeling of the 1992 Landers earthquake. *Journal of Geophysical Research* 106: 26467–26482.
- Poliakov AB, Dmowska R, and Rice JR (2002) Dynamic shear rupture interactions with fault bends and off-fault secondary faulting. *Journal of Geophysical Research* 107. <http://dx.doi.org/10.1029/2001JB000572>.
- Power WL and Tullis TE (1995) A review of the fractal character of natural fault surfaces with implications for friction and the evolution of fault zones. In: Barton CC and LaPointe PR (eds.) *Fractals in the Earth Sciences*, pp. 89–105. New York: Plenum.
- Reches Z and Lockner DA (2010) Fault weakening and earthquake instability by powder lubrication. *Nature* 467. <http://dx.doi.org/10.1038/nature09348> (452-U102).
- Reid H (1910) The mechanism of the earthquake. In: Comm RSI (ed.). *The California Earthquake of April 19, 1906*, vol. 2. Washington, DC: Carnegie Institution.
- Rice JR (1968a) Mathematical analysis in the mechanics of fracture. In: Liebowitz H (ed.). *Fracture: An Advanced Treatise*, vol. 2, pp. 191–311. New York: Academic Press.
- Rice JR (1968b) A path-independent integral and the approximate analysis of strain concentration by notches and cracks. *Journal of Applied Mechanics* 35: 379–386.
- Rice JR (1979) The mechanisms of quasistatic crack growth. In: Kelly RE (ed.) *Proceedings of 8th US National Congress on Applied Mechanics, UCLA, June 1978*, pp. 191–216. North Hollywood, CA: Western Periodicals.
- Rice JR (1980) The mechanics of earthquake rupture. In: Dziewonski AM and Boschi E (eds.) *Physics of the Earth's Interior*, pp. 555–649. Amsterdam: North-Holland.
- Rice JR (1993) Spatio-temporal complexity of slip on a fault. *Journal of Geophysical Research* 98: 9885–9907.
- Rice JR (2006) Heating and weakening of faults during earthquake slip. *Journal of Geophysical Research* 111: B05,311.
- Rice JR, Sammis CG, and Parsons R (2005) Off-fault secondary failure induced by a dynamic slip pulse. *Bulletin of the Seismological Society of America* 95: 109–134.
- Richards P (1976) Dynamic motions near an earthquake fault – 3-dimensional solution. *Bulletin of the Seismological Society of America* 66: 1–32.
- Rivera LA and Kanamori H (2005) Representations of the radiated energy in earthquakes. *Geophysical Journal International* 162: 148–155.
- Rogers G and Dragert H (2003) Episodic tremor and slip on the Cascadia subduction zone: The chatter of silent slip. *Science* 300: 1942.
- Rubin AM (1993) Tensile fracture of rock at high confining pressure: Implications for dike propagation. *Journal of Geophysical Research* 98: 15919–15935.
- Rubin AM and Ampuero J-P (2005) Earthquake nucleation on (aging) rate and state faults. *Journal of Geophysical Research* 110: B11,312. <http://dx.doi.org/10.1029/2005JB003686>.
- Rudnicki JW (1980) Fracture mechanics applied to the Earth's crust. *Annual Review of Earth and Planetary Sciences* 8: 489–525.
- Rudnicki JW and Freund LB (1981) On energy radiation from seismic sources. *Bulletin of the Seismological Society of America* 71: 583–595.
- Ruina A (1983) Slip instability and state variable friction laws. *Journal of Geophysical Research* 88: 10359–10370.
- Samudrala O, Huang Y, and Rosakis AJ (2002) Subsonic and intersonic shear rupture of weak planes with a velocity weakening cohesive zone. *Journal of Geophysical Research* 107: B2170. <http://dx.doi.org/10.1029/2001JB000460>.
- Savage J (1998) Displacement field for an edge dislocation in a layered half-space. *Journal of Geophysical Research* 103: 2439–2446.
- Scholz CH (1998) Earthquakes and friction laws. *Nature* 391: 37–42.
- Scholz CH (2002) *The Mechanics of Earthquakes and Faulting*, 2nd edn, p. 496. New York, NY: Cambridge University Press.
- Segall P (1991) Fault mechanics. *Reviews of Geophysics* 29: 864–876.
- Segall P and Rice JR (1995) Dilatancy, compaction, and slip instability of a fluid infiltrated fault. *Journal of Geophysical Research* 100: 22155–22171.
- Sibson RH (1973) Interaction between temperature and pore-fluid pressure during earthquake faulting – A mechanism for partial or total stress relief. *Nature* 243: 66–68.
- Sibson RH (1975) Generation of pseudotachylite by ancient seismic faulting. *Geophysical Journal of the Royal Astronomical Society* 43: 775–794.
- Sibson R (1980) Power dissipation and stress levels on faults in the upper crust. *Journal of Geophysical Research* 85: 6239–6247.
- Simonov IV (1983) Behavior of solutions of dynamic problems in the neighborhood of the edge of a cut moving at transonic speed in the elastic medium. *Mechanics of Solids (Mekhanika Tverdogo Tela)* 18: 100–106.
- Spray JG (2005) Evidence for melt lubrication during large earthquakes. *Geophysical Research Letters* 32. <http://dx.doi.org/10.1029/2004GL022293>, Art. No. L07,301.
- Steketee JA (1958) Some geophysical applications of the elasticity theory of dislocations. *Canadian Journal of Physics* 36: 1168–1198.
- Swanson MP (1992) Fault structure, wear mechanisms and rupture processes in pseudotachylite generation. *Tectonophysics* 204: 223–242.
- Takeuchi C and Fialko Y (2012) Dynamic models of interseismic deformation and stress transfer from plate motion to continental transform faults. *Journal of Geophysical Research* 117: B05,403. <http://dx.doi.org/10.1029/2011JB009056>.
- Timoshenko S and Goodier JN (1970) *Theory of Elasticity*, 3rd edn. New York: McGraw-Hill, 398 pp.
- Tinti E, Spudich P, and Cocco M (2005) Earthquake fracture energy inferred from kinematic rupture models on extended faults. *Journal of Geophysical Research* 110: B12,303. <http://dx.doi.org/10.1029/2005JB003644>.
- Tsutsumi A and Shimamoto T (1997) High-velocity frictional properties of gabbro. *Geophysical Research Letters* 24: 699–702.
- Vvedenskaya AV (1959) Determination of displacement fields for earthquakes by means of the dislocation theory. *Izvestiya Akademii nauk SSSR; Seriya geofizicheskaya* 3: 277–284 (in Russian).
- Wald DJ and Heaton TH (1994) Spatial and temporal distribution of slip for the 1992 Landers, California, earthquake. *Bulletin of the Seismological Society of America* 84: 668–691.
- Wenk H-R, Johnson L, and Ratschbacher L (2000) Pseudotachylites in the Eastern Peninsular Ranges of California. *Tectonophysics* 321: 253–277.
- Westergaard H (1939) Bearing pressures and cracks. *Journal of Applied Mechanics, Transactions of the ASME* 6: A49–A53.
- Willis JR (1967) A comparison of the fracture criteria of Griffith and Barenblatt. *Journal of the Mechanics and Physics of Solids* 15: 151–162.
- Wilson B, Dewers T, Reches Z, and Brune J (2004) Particle size and energetics of gouge from earthquake rupture zones. *Nature* 434: 749–752.
- Xia K, Rosakis AJ, and Kanamori H (2004) Laboratory earthquakes: The sub-Rayleigh-to-super-shear rupture transition. *Science* 303: 1859–1861.
- Zheng G and Rice J (1998) Conditions under which velocity-weakening friction allows a self-healing versus a cracklike mode of rupture. *Bulletin of the Seismological Society of America* 88: 1466–1483.